NASA CR-165,485

NASA CR-165485

NASA-CR-165485
1982 0003007

# EXPERIMENTAL SIMULATION OF THE INTERACTION OF BIASED SOLAR ARRAYS WITH THE SPACE PLASMA

Prepared for

LEWIS RESEARCH CENTER

NATIONAL AERONAUTICS AND SPACE ADMINISTRATION

GRANT NSG 3196

LIBRARY COPY

NOV 12 1981

LANGLEY RESEARCH CENTER
LIBRARY, NASA
HAMPTON, VIRGINIA

Annual Report

May 1981

Harold R. Kaufman and Raymond S. Robinson
Department of Physics
Colorado State University
Fort Collins, Colorado

NF01580

| 1. Report No. | 2. Government Accession No. | 3. Recipient's Catalog No. |
|---|---|---|
| CR-165485 | | |

| 4. Title and Subtitle | 5. Report Date |
|---|---|
| Experimental Simulation of Interaction of Biased Solar Arrays with the Space Plasma | May 1981 |
| | 6. Performing Organization Code |
| 7. Author(s) | 8. Performing Organization Report No. |
| Harold R. Kaufman and Raymond S. Robinson | Annual Report |
| 9. Performing Organization Name and Address | 10. Work Unit No. |
| Department of Physics<br>Colorado State University<br>Fort Collins, Colorado 80523 | 11. Contract or Grant No.<br>NSG-3196 |
| 12. Sponsoring Agency Name and Address | 13. Type of Report and Period Covered |
| NASA Lewis Research Center<br>21000 Brookpark Road<br>Cleveland, OH 44135 | 14. Sponsoring Agency Code<br>5532 |

15. Supplementary Notes

Grant Manager: Norman T. Grier
NASA Lewis Research Center
Cleveland, OH 44135

16. Abstract


The operation of high voltage solar arrays in the space environment can result in anomalously large currents being collected through small insulation defects. Understanding this phenomenon is the objective of this research program.

Polyimide (Kapton) was the insulating material used in all tests. Both positive bias (electron collection) and negative bias (ion collection) tests were conducted.

Negative bias tests indicated two regimes of ion collection. In the lower voltage regime collected currents were of the magnitude expected from electrostatic collection. In the higher voltage regime collected currents were higher than expected from electrostatic collection, but still considerably lower in magnitude than those collected with positively biased conductors. In the higher collection regime a brownish layer was deposited on the conductor, suggesting vaporization or sputtering of the insulating material occurs.

Positive bias tests were done for high current collection (up to 5 mA). It was found that a mode change in the electron collection mechanism occurs at high currents. This mode change is associated with a glow discharge process and was found to be related to the neutral background density. Results indicated that the glow discharge collection mode would not occur in a space environment where the neutral background density is considerably lower than that of the vacuum facility used.

Some modeling for electron collection was done. The model assumed secondary electron emission as the major collection mechanism and a plasma sheath covering an effective collection area. Calculations showed that the assumption of a planar sheath is incorrect and that a hemispherical sheath covering a much larger area than the collection area is indicated.


| 17. Key Words (Suggested by Author(s)) | 18. Distribution Statement |
|---|---|
| Plasma Physics<br>Space Plasma<br>Solar Arrays | Unclassified - Unlimited |

| 19. Security Classif. (of this report) | 20. Security Classif. (of this page) | 21. No. of Pages | 22. Price* |
|---|---|---|---|
| Unclassified | Unclassified | | |

* For sale by the National Technical Information Service, Springfield, Virginia 22161

NASA-C-168 (Rev. 10-75)

N82-10880#

TABLE OF CONTENTS


| | | Page |
|---|---|---|
| I. | INTRODUCTION | 1 |
| II. | APPARATUS AND PROCEDURE | 3 |
| | Vacuum Facility | 3 |
| | Solar Array Simulation | 3 |
| | Procedure | 4 |
| III. | EXPERIMENTAL RESULTS | 5 |
| | Positive Bias - Electron Collection | 5 |
| | Normalization | 5 |
| | Effect of Insulator Area | 5 |
| | High Current Measurements | 7 |
| | Effect of Hole Size at High Current Measurements | 11 |
| | Multiple Holes | 11 |
| | Negative Bias - Ion Collection | 13 |
| | Variation of Current Collection with Time | 14 |
| IV. | MODELING | 18 |
| | Collection Area | 18 |
| | Electron Trajectories Across the Insulator Surface | 26 |
| | Surface Charge Density | 26 |
| | Surface Potential | 27 |
| | Electric Field Along the Surface | 30 |
| | Sample Calculations | 32 |
| | Electric Field Above the Surface | 32 |
| | Equations of Motion | 35 |
| V. | CONCLUDING REMARKS | 43 |

APPENDIX A..... 44

APPENDIX B..... 54

REFERENCES..... 61

DISTRIBUTION..... 65

LIST OF FIGURES


| | | Page |
|---|---|---|
| Fig. 3-1. | Comparison of samples with different insulator surface areas | 6 |
| Fig. 3-2. | Electron current collection characteristics extended to higher currents | 8 |
| Fig. 3-3. | Hole power at mode change versus neutral density | 10 |
| Fig. 3-4. | Current collection as a function of time for a bias of -4500 volts | 17 |
| Fig. 4-1. | Schematic of electron collection model | 19 |
| Fig. 4-2. | Power of temperature variation for electron current as a function of conductor potential | 21 |
| Fig. 4-3. | Insulator collection radius as a function of conductor potential | 23 |
| Fig. 4-4. | Comparison of experimental and calculated electron current collection characteristics for a hole diameter of 1 mm, electron density of $7.4 \times 10^5$ $cm^{-3}$, electron temperature of 7.7 eV and conductor temperature of 320°K | 24 |
| Fig. 4-5. | Comparison of experimental and calculated electron current collection characteristics for a hole diameter of 0.52 mm, electron density of $2.1 \times 10^5$ $cm^{-3}$, electron temperature of 12.8 eV and conductor temperature of 313°K | 25 |
| Fig. 4-6. | Normalized surface charge density as a function of normalized radius | 28 |
| Fig. 4-7. | Normalized surface potential as a function of normalized radius | 29 |
| Fig. 4-8. | Normalized electric field along the surface as a function of normalized radius | 33 |
| Fig. 4-9. | The (a) surface charge density, (b) surface potential, and (c) electric field along the surface plotted against normalized radius for an applied conductor potential of 601 volts | 34 |
| Fig. 4-10. | Two possible electric fields above the surface as a function of normalized radius for conductor potential of 601 volts | 36 |

Fig. 4-11. Electron trajectories for an electron moving across the insulator for $E_z$ calculated from (a) the surface charge density and (b) Child's law, for a conductor potential of 601 volts and initial velocity equivalent to 2 eV normal to the surface.... 39

Fig. 4-12. Normalized sheath thickness, for Child's law sheath, as a function of normalized radius for a conductor potential of 601 volts..... 41

Fig. 4-13. Schematic of proposed model with hemispherical sheath..... 42

Fig. B-1. (a) Total yield from Willis and Skinner[4] and (b) secondary electron yield from Leung, Tueling and Schnauss[5] as a function of incident electron energy..... 55

Fig. B-2. Energy distribution of secondary electrons emitted by tantalum[9]..... 58

LIST OF TABLES

Page

Table 3-1. Results of neutral density tests involving mode change point..... 9

Table 3-2. Results of various hole diameters at high currents... 12

Table 3-3. Conductor potentials where ion current collection first exceeded 100 μA, for various size holes..... 15

Table 4-1. Collection radius, collected current, current density, surface velocity and normalized hole radius for various values of conductor potential..... 31

# I. INTRODUCTION

Solar cell arrays constitute the major source of reliable long-term power for spacecraft orbiting the earth. High voltage solar arrays are desired to optimize both spacecraft mass and power efficiency. The space plasma environment,[1-3] though, can result in large currents being collected by exposed solar cells, with corresponding reductions in power output from the array. The obvious solution of using a covering of transparent insulation is at least partially offset by the expectation of defects, either from the manufacturing process or resulting from collisions with micrometeors. Early experiments showed that positive electrodes behind pinhole openings in the insulating sheets could collect electron currents far in excess of what would be expected from electrostatic theory.[4] Subsequent investigators verified these large currents, but showed a wide range of results, depending on materials, configuration, and operating conditions used in the tests.[5-8]

The purpose of this research is to investigate the phenomenon of unexpectedly large leakage currents collected by small exposed areas of high voltage solar arrays operating in a plasma environment used to simulate space. This report covers the progress since the last annual report.[9] The results of the two previous annual reports[9-10] and some of the material for this support period is reviewed in the paper of Appendix A.[11]

The experimental research done during the present grant period involved only one type of insulating material, polyimide (Kapton). Positive bias tests (relative to the plasma) were done studying the glow discharge mode of current collection.[9] Tests were performed

studying the transition from space-charge flow current collection to current collection well above space charge flow values. Variation of current collection with time was also investigated.

Some modeling for electron collection was done. This involved some numerical solutions, but is not a detailed computer simulation of the phenomenon as others are attempting.[12]

Appendix B is a summary of some of the properties of secondary electron emission from insulators. Several of these properties have been mentioned in previous reports[9-10] and some are included for possible use in future modeling of electron collection.

# II. APPARATUS AND PROCEDURE

## Vacuum Facility

The experiments were conducted in a 45 cm diameter, 72 cm long cylindrical vacuum system. An argon hollow cathode mounted horizontally at the base of the vacuum system was used to generate the plasma. The hollow cathode supplied electrons which then ionized the argon. The only source of argon gas in the vacuum system was the flow through the hollow cathode. This is the same configuration used previously.[1]

The operating pressure in the vacuum system was in the range of $9\text{-}100 \times 10^{-5}$ Torr. The electron temperature ranged from 3.2 to 7.9 eV and the plasma density ranged from $1\text{-}26 \times 10^{5}$ $cm^{-3}$. The range of plasma parameters approximates the environments expected for both an electrically propelled spacecraft, due to its own charge exchange plasma[2] and a spacecraft in a natural low earth orbit plasma environment.[3] Measurements of the plasma characteristics were taken with a spherical Langmuir probe. The measurement techniques have been described in detail elsewhere.[4]

## Solar Array Simulation

The insulated array of solar cells were simulated by placing a sheet of insulating material (polyimide) over a conductor. The sheet of polyimide was held to the conductor by a pressure sensitive adhesive (Y966 by 3M). A small hole was punched into the insulating sheet and adhesive to simulate the defect. A heater and thermocouple were attached to the conductor. This permitted the control and measurement of the conductor temperature. A more detailed description is given in the previous report.[1]

## Procedure

The simulated solar cell was centrally and vertically mounted in the vacuum system. A plasma was generated and the temperature of the sample adjusted to the desired setting (room temperature, 300°K, unless otherwise specified). The sample was then bombarded by the plasma for at least one hour to stimulate desorption of gases on the insulator surface. A slowly increasing voltage was applied to the conductor, while the current collected through the hole was monitored along with the conductor potential. Langmuir probe characteristics were taken for determination of plasma properties after each test. Using known correlations, the plasma properties are set to approximately the desired values before each test. Test variables included: hole diameter, polyimide thickness, conductor temperature, background pressure, and voltage magnitude and polarity.

# III. EXPERIMENTAL RESULTS

R. P. Stillwell

## Positive Bias - Electron Collection

Normalization. The current/voltage data has been normalized by dividing the total hole current by the random current density,[1]

$$j_o = \frac{1}{4} en \sqrt{\frac{8kT_e}{\pi m_e}} \tag{3-1}$$

where e is the magnitude of the electronic charge, n is the electron density, k is Boltzmann's constant, $T_e$ is the electron temperature, and $m_e$ is the electron mass. All values are in SI units, unless otherwise specified. This normalization was found to successfully eliminate scatter in the data due to electron density and temperature differences as reported previously.[2]

Effect of Insulator Area. In the first support period,[3] data were taken using different insulator areas. These data were presented in a logarithmic current plot, and it was concluded that there the anticipated strong effect of area was not evident. The tests used three sample sizes: 2 × 2 cm, 5 × 5 cm, and 12 × 12 cm. These samples gave a surface area range of 4 $cm^2$ to 144 $cm^2$. The results of these tests are again shown in Fig. 3-1. From this linear plot, it is seen that some area effect is evident. The effect shown in Fig. 3-1, though, is considerably smaller than that found in an earlier investigation.[4] The normalized results shown lie within the extremes of the data of the earlier investigation, which exhibit a much steeper rise in current collection with increased insulator area surrounding the hole. The difference is possibly due to differences in experimental conditions. The earlier investigation used a directed ion beam composed of nitrogen for the

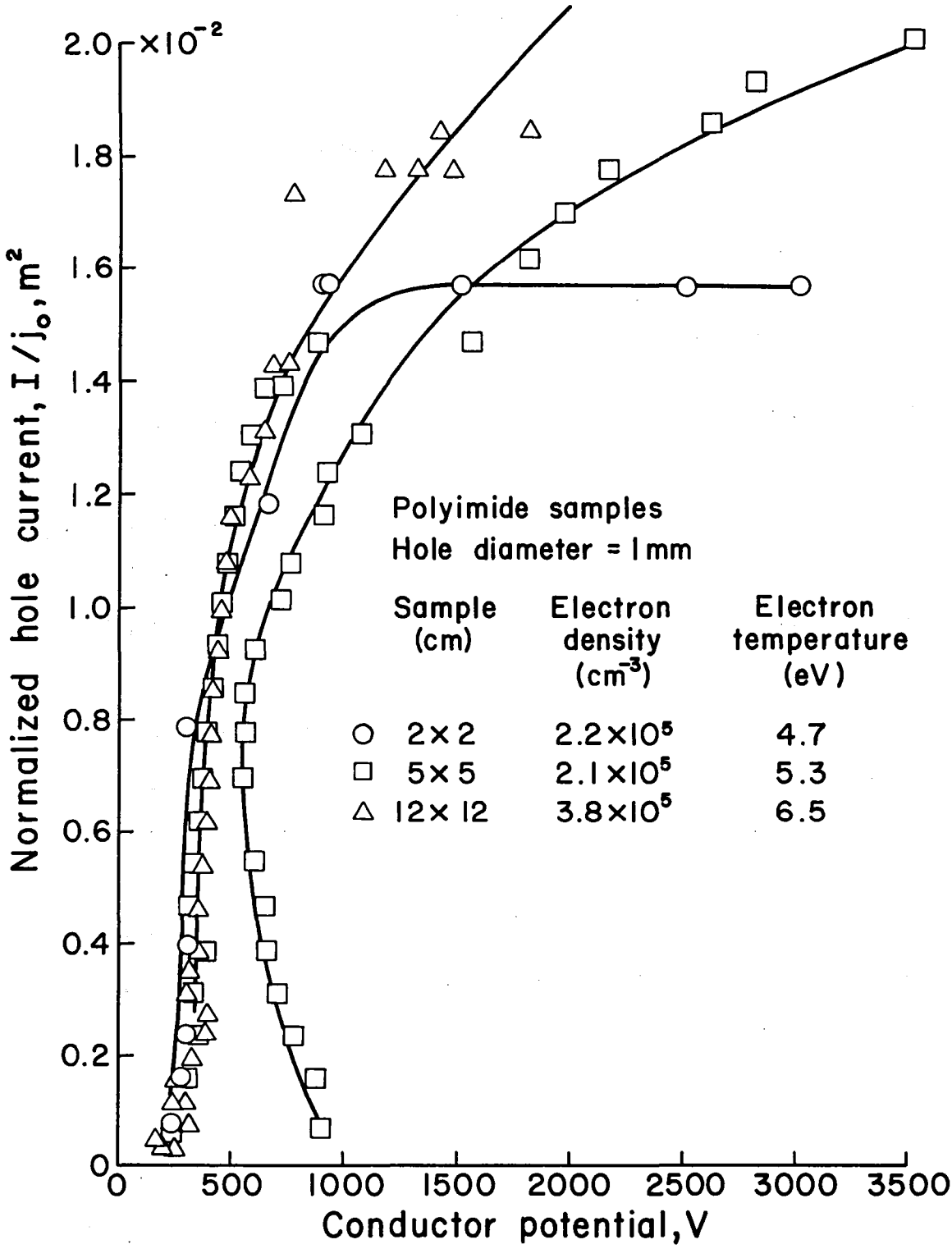


Fig. 3-1. Comparison of samples with different insulator surface areas.

plasma source, an electron density of 2-17 × $10^3$ $cm^{-3}$ and a background pressure range of 1-10 × $10^{-5}$ Torr. These conditions differed from the environment used herein (see Section II).

The double-valued curve in Fig. 3-1 for the 5 × 5 cm sample is not completely understood; although this behavior is not typical, it is felt to be due primarily to lack of regulation in the high voltage power supply.

High Current Measurements. As reported previously,[2] in collecting high currents, up to 5 mA, there appears to be a change in collection modes, indicated by the dashed lines in Fig. 3-2. The mode change that occurs at 1.5 mA in Fig. 3-2 is characteristic of high current measurements. During tests a bluish glow was observed to increase in intensity and extent with this change in mode. From these observations, a possible explanation for the mode change is a glow discharge initiation involving background neutrals. The mode change that occurs at approximately 0.25 mA in Fig. 3-2 is less intense than the mode change at 1.5 mA. It also is unusual in that all other mode changes observed were associated with luminosity changes. The lower mode change (0.25 mA) does not have a glow associated with it, and is as yet unexplained. The data taken after the first mode change (0.25 mA) are still in rough agreement with the data taken by Kennerud,[4] indicating that any glow discharge effect below the glow discharge mode is probably negligible.

Tests were performed to determine if there is any relation between the glow discharge observed at high currents and the background neutral density. The results are presented in Table 3-1. The data of Table 3-1 indicates that the hole power (collected current times conductor potential) at the mode change (occurs at 1.5 mA in Fig. 3-2) increases with decreasing neutral density, shown in Fig. 3-3. Below about

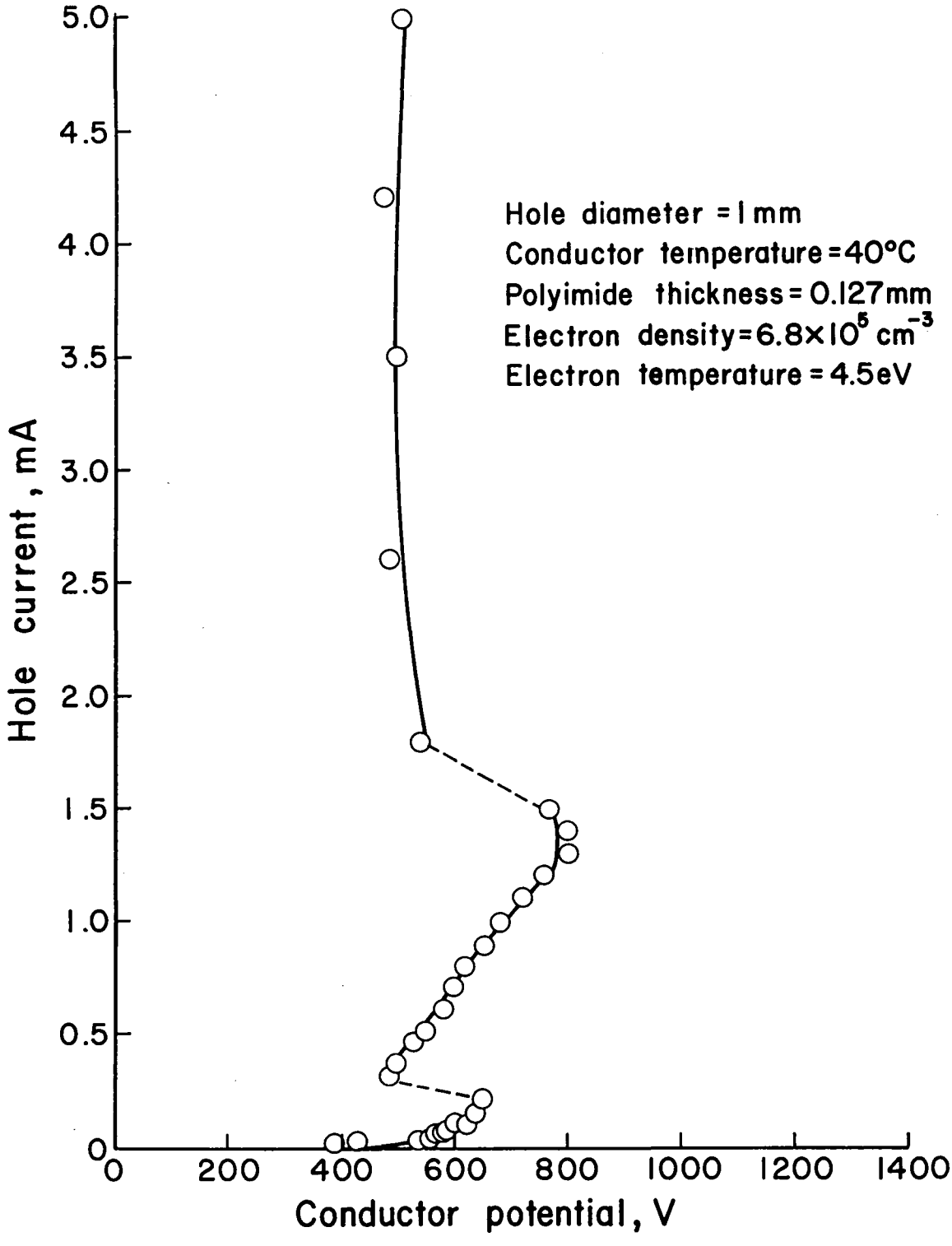


Fig. 3-2. Electron current collection characteristics extended to higher currents.

Table 3-1. Results of Neutral Density Tests Involving Mode Change Point.

| Neutral Density ($cm^{-3}$) | Conductor Potential at Mode Change (volts) | Collected Current at Mode Change ($\mu A$) | Electron Density ($cm^{-3}$) |
|---|---|---|---|
| $2.9 \times 10^{12}$ | 850 | 3000 | $5.6 \times 10^{5}$ |
| $3.2 \times 10^{12}$ | 770 | 4200 | - |
| $4.0 \times 10^{12}$ | 790 | 290 | - |
| $9.7 \times 10^{12}$ | 510 | 270 | $1.8 \times 10^{6}$ |
| $1.6 \times 10^{13}$ | 565 | 190 | $1.2 \times 10^{5}$ |
| $1.9 \times 10^{13}$ | 485 | 110 | $2.2 \times 10^{5}$ |
| $2.4 \times 10^{13}$ | 445 | 145 | $1.5 \times 10^{5}$ |
| $3.2 \times 10^{13}$ | 480 | 125 | $2.6 \times 10^{6}$ |

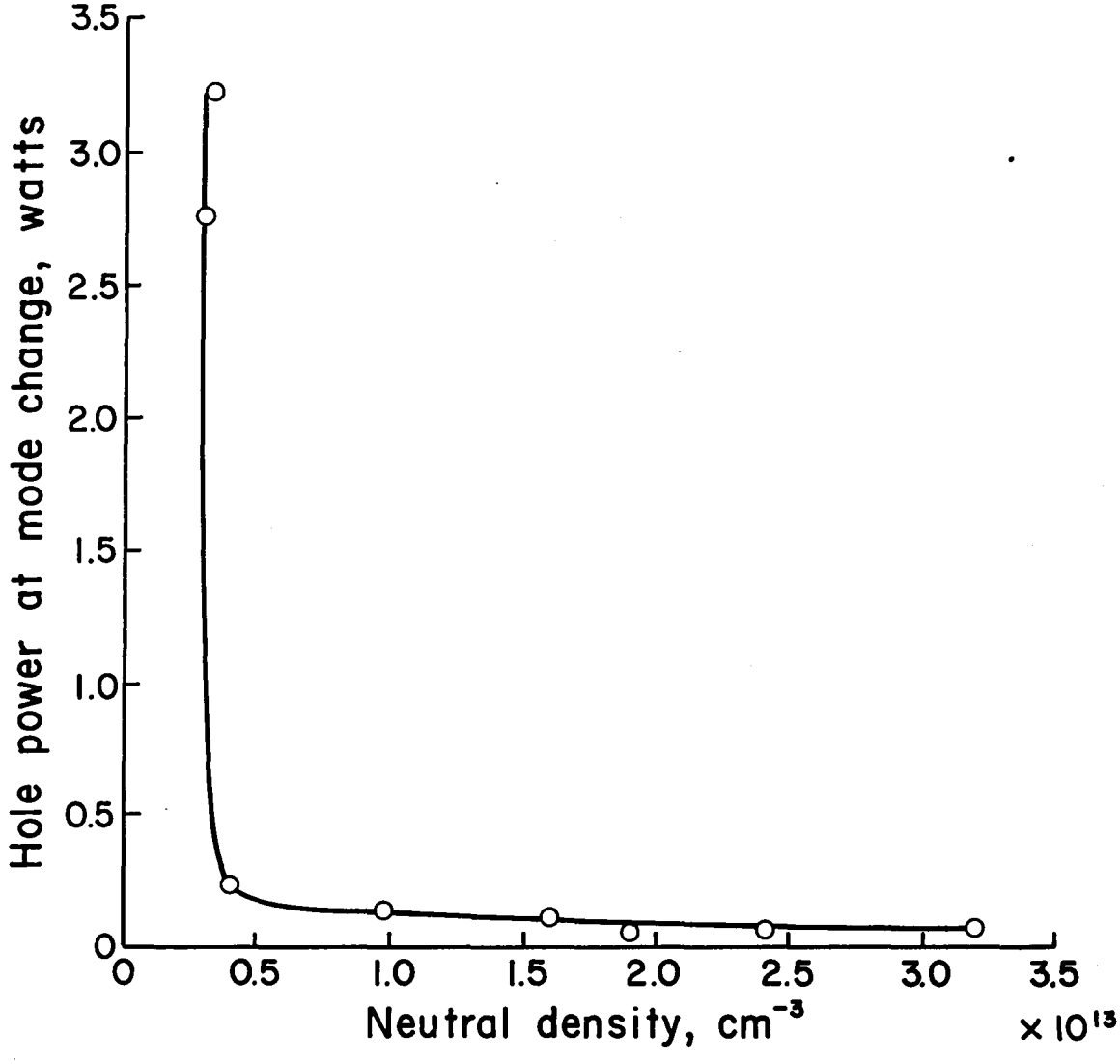


Fig. 3-3. Hole power at mode change versus neutral density.

$3 \times 10^{12}$ neutrals/cm$^3$, the required power rises to high values. The glow discharge process would then not be expected to occur in space where much lower neutral densities are found. Future tests should then be performed in an environment with a significantly lower neutral density than is presently used, preferably below $3 \times 10^{12}$/cm$^3$.

Effect of Hole Size at High Current Measurements. Studies were done to determine if current collection at high currents was affected by hole size. Five hole diameters were tested; 1.0 mm, 2.0 mm, 3.0 mm, 4.1 mm, and 5.0 mm. The results of these tests are presented in Table 3-2. The current/voltage curves did not correlate well when using the random current density factor, $j_o$, nor did they correlate well when using the factor of random current times hole area ($I_o = j_o \times$ hole area). However, if the conductor potential at a current of 1.5 mA is evaluated, it is seen that the potential at this current decreases with increasing hole size. This result suggests that hole size is an important parameter for collection at high currents in the absence of a glow discharge collection mode. The conductor potential at 5 mA is shown in Table 3-2. (The 5 mA data corresponded to a glow discharge in all cases.) No correlation was found among hole size, electron density and current collection in the glow discharge mode.

These tests indicate that further studies of hole size versus high current collection, in the absence of a glow discharge collection mode, are necessary.

Multiple Holes. During tests, when the laboratory was darkened, small localized bluish glows were observed around the holes prior to the mode change (glow discharge mode). To study these glows further, experiments were done in which two 1 mm diameter holes were punched in the polyimide. Two tests were performed in which the holes were

Table 3-2. Results of Various Hole Diameters at High Currents.

| Hole Diameter (mm) | Electron Density ($cm^{-3}$) | Electron Temperature (eV) | Neutral Density ($cm^{-3}$) | Conductor Potential at 1.5 mA (volts) | Conductor Potential at 5 mA (volts) |
|---|---|---|---|---|---|
| 1.0 | $1.3 \times 10^{6}$ | 6.1 | $8.0 \times 10^{12}$ | 860 | 440 |
| 2.0 | $5.7 \times 10^{5}$ | 5.7 | $9.7 \times 10^{12}$ | 720 | 1050 |
| 3.0 | $1.5 \times 10^{6}$ | 5.5 | $9.7 \times 10^{12}$ | 500 | 2200 |
| 4.1 | $1.1 \times 10^{6}$ | 4.6 | $9.7 \times 10^{12}$ | 335 | 1900 |
| 5.0 | $1.1 \times 10^{6}$ | 3.2 | $9.7 \times 10^{12}$ | 320 | 730 |

separated by 2 cm and 5 cm (center to center). The results show no interaction between holes when the glows are first observed, as indicated by measurements of total power, neutral density or electron density.

The glows became visible in both holes at the same time. Otherwise, they appear to be independent of each other. The glows differed in both intensity and extent in each hole. With increasing current, the glows gradually grew until they merged with each other. This occurred at 0.33 watts (510 volts) for the 2 cm hole separation and at 1.10 watts (1100 volts) for the 5 cm hole separation. Once merged, the glow continued to expand outward.

During the tests, arcs were also visible in the holes. The arcs in each hole also appeared to be independent. These arcs were not always visible, disappearing and returning in an apparently random fashion. The arcs appeared to be red at first, then becoming white. The arcs in the holes continued even after the glows merged.

## Negative Bias - Ion Collection

It was previously reported[2] that for negative conductor potentials under a 1000-volt magnitude, collected currents agreed with values predicted from electrostatic theory. Tests were conducted at larger voltages. These tests were done with five different hole diameters; 1.0 mm, 2.0 mm, 3.0 mm, 4.1 mm and 5.0 mm. The tests all yielded the same qualitative results.

At negative potentials greater than about 1000 V, the current began to oscillate. These oscillations appeared to become larger with both time and voltage. During these oscillations, localized arcing was observed around the hole. As the current increased, this arcing

appeared more continuous and the current collection became more steady. The currents measured at this point were usually between 100 and 200 μA. Tests were stopped at about the 100-200 μA level because arcing was observed between the high voltage connector leading to the sample and the sample holder. This was typically at negative potentials greater than 5000 V.

From these results there appear to be two regimes of current collection. In the lower voltage regime collected currents are of the magnitude expected from electrostatic collection. In the higher voltage regime collected currents are much higher than expected from electrostatic collection, although still considerably lower in magnitude than those collected with positively biased conductors. This higher collection regime appears to be associated with arcing occurring in the hole. It has also been observed that a dark brownish layer is deposited on the conductor exposed to the plasma by the hole. This suggests that the polyimide is vaporized or sputtered. The transition between these two regimes is very unsteady and is characterized by large current oscillations and to a smaller extent by voltage oscillations. That is, when the arcing appears continuous, the current rises and voltage decreases.

Variation of Current Collection with Time. Tests measuring current collection as a function of time, at constant negative potential, were performed. These tests were conducted to determine if the dark brownish layer deposited on the conductor affected the ion collection.

The criterion used to determine the voltage for these tests was the voltage value when a hole began collecting more than 100 μA. This value was chosen because 100 μA is in the high current collection regime. Table 3-3 shows the data from which the voltage for these tests was determined. The tabulated values of voltage do not show a consistant

Table 3-3. Conductor Potentials where Ion Current Collection First Exceeded 100 μA, for Various Size Holes.

| Hole Diameter (mm) | Conductor Potential for Collection ≥100 μA (volts) |
|---|---|
| 1.0 | -6100 |
| | -3100 |
| | -5100 |
| 2.0 | -3800 |
| 3.0 | -5500 |
| | -3600 |
| 4.1 | -4100 |
| 5.0 | -4400 |

trend with hole diameter. The average of all values in Table 3-3 is about -4500 volts. This value (-4500 v) was therefore used in these tests.

Three hole diameters were tested; 0.35, 3.0 and 5.0 mm. These three hole sizes cover the range of hole sizes used to date.

Figure 3-4 shows the results of these tests. It was observed during these tests that the decrease in collected current roughly corresponds to the development of the brownish film.

During these tests there was also considerable voltage/current oscillation (see Fig. 3-4). This indicates the need for a regulated power supply in future tests.

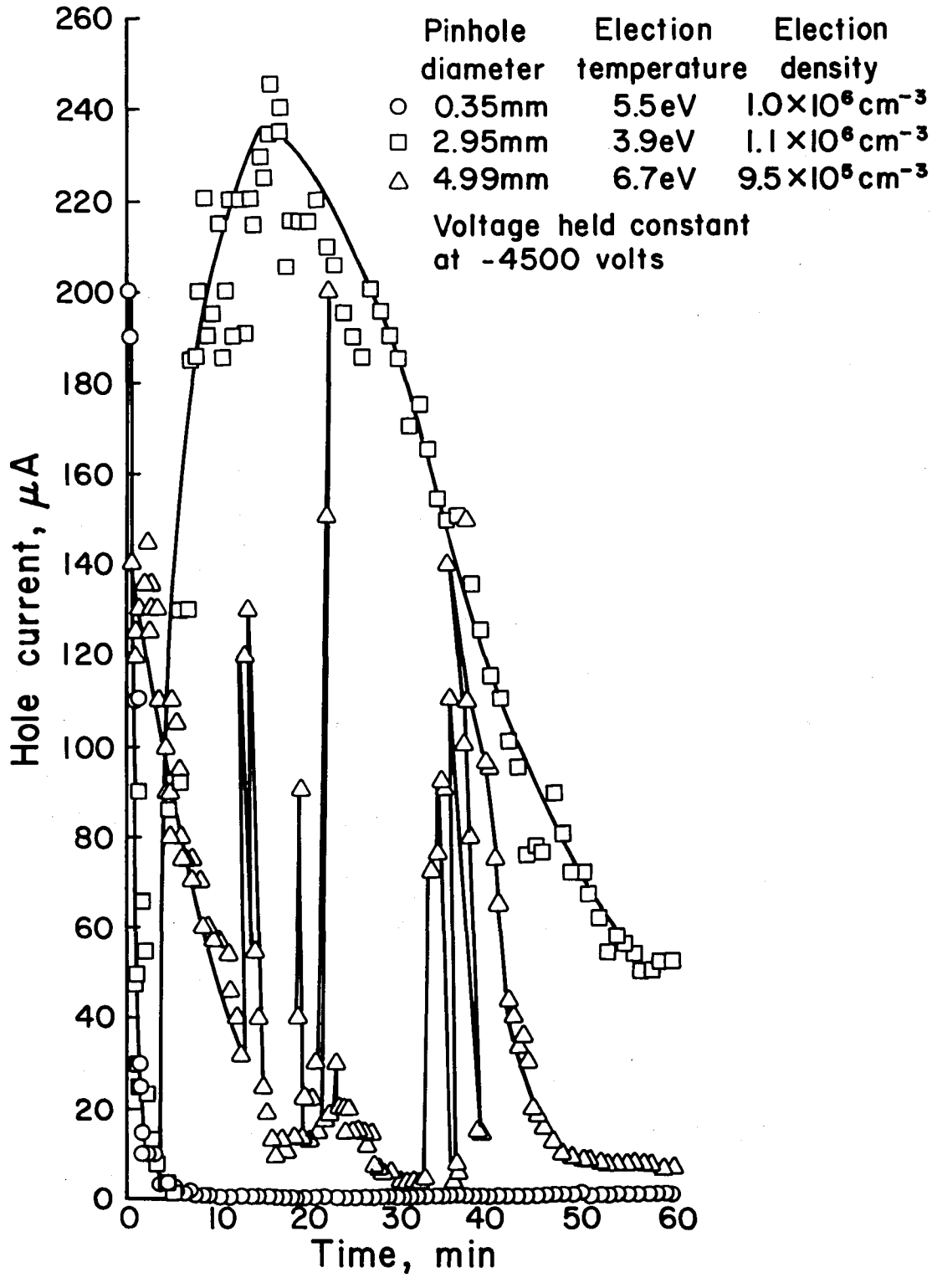


Fig. 3-4. Current collection as a function of time for a bias of -4500 volts.

# IV. MODELING

R. P. Stillwell

For positive bias (electron collection), the approach taken has been that part of the insulator surrounding the exposed conductor (the hole) takes part in the current collection. The mechanism for the electrons moving across the insulator material to the hole, for collection by the conductor, is taken to be secondary electron emission. The driving force for this process is a potential gradient from the hole (at applied conductor potential) to some radius on the insulator (near floating potential) which does not contribute to the electron collection.

The process envisioned is an electron from the plasma striking the surface of the insulator, within the collection radius, and a secondary electron being emitted. This secondary electron, moving in a direction toward the hole, gains energy from the potential gradient and strikes the surface with sufficient energy to cause another secondary electron to be emitted. In this manner, an electron striking the insulator, within the collection area, appears to travel across the surface to the hole. The secondary electron emission coefficient would have to be unity, on the average, for the traveling electrons to maintain current continuity and conservation of charge.

In this approach, the sheath would essentially cover only the area of the insulator contributing to the electron collection. This model is visualized in Fig. 4-1. In the figure, $r_h$ represents the radius of the hole while $r_c$ represents the total collection radius.

## Collection Area

The first calculations done were to determine if the model was feasible on the basis of the necessary size of the collection radius, $r_c$.

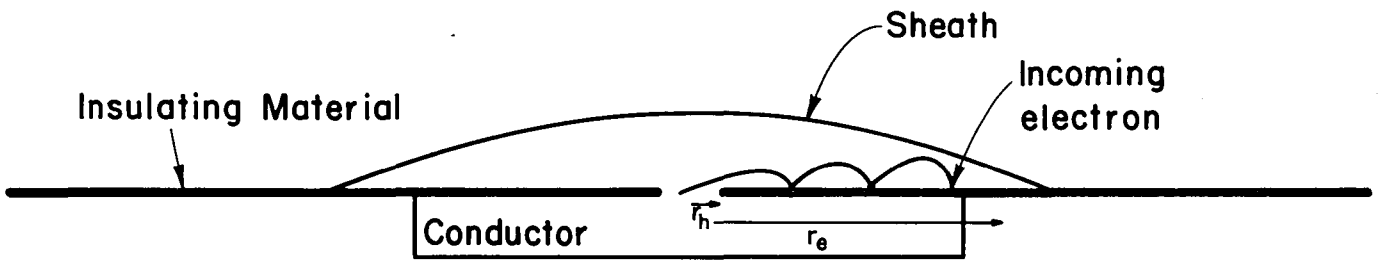


Fig. 4-1. Schematic of electron collection model.

The current is given by the expression

$$I = j_o \left[1 + \frac{b^2}{4} + (1 - \frac{b^2}{4}) \frac{eV_a}{kT_e}\right] \left[A_h + A_i \left(\frac{298}{T}\right)^{\xi(V_a)}\right] \tag{4-1}$$

The term $j_o\{1 + b^2/4 + (1 - b^2/4)\ eV_a/kT_e\}$ is the collection term found by Parker and Whipple for collection by a planar probe surrounded by a grounded conductor.[1] The b in this term is a constant, found to be about 1.8 for the test environment used herein.[2] $V_a$ is the applied conductor potential, k is Boltzmann's constant, $T_e$ is the electron temperature, e is the electronic charge, and $j_o$ is the random current density, given by[3]

$$j_o = \frac{1}{4}\ ne\sqrt{\frac{8kT_e}{\pi m_e}} \tag{4-2}$$

where n is the electron density and $m_e$ the electronic mass. The term $\{1 + b^2/4 + (1 - b^2/4)\ eV_a/kT_e\}$ represents the geometry factor associated with the expanding sheath. The area is given by the term $\{A_h + A_i\ (298/T)^{\xi(V_a)}\}$. $A_h$ is the area of exposed conductor, $A_i$ the area of insulating material contributing to the electron collection, and T is the sample temperature (in °K). The area $A_i$ is multiplied by the factor $(298/T)^{\xi(V_a)}$ to take into account the temperature dependence cf the collected current[4] (also see Appendix B). The temperature term is not multiplied by the total collection area because only the collection by the insulator is affected by the sample temperature. The expression for $\xi(V_a)$ was the best linear least squares fit to the experimental data[4] (see Fig. 4-2). It was found to be

$$\xi(V) = 2.1 + 4.3 \times 10^{-3}\ V_a\ . \tag{4-3}$$

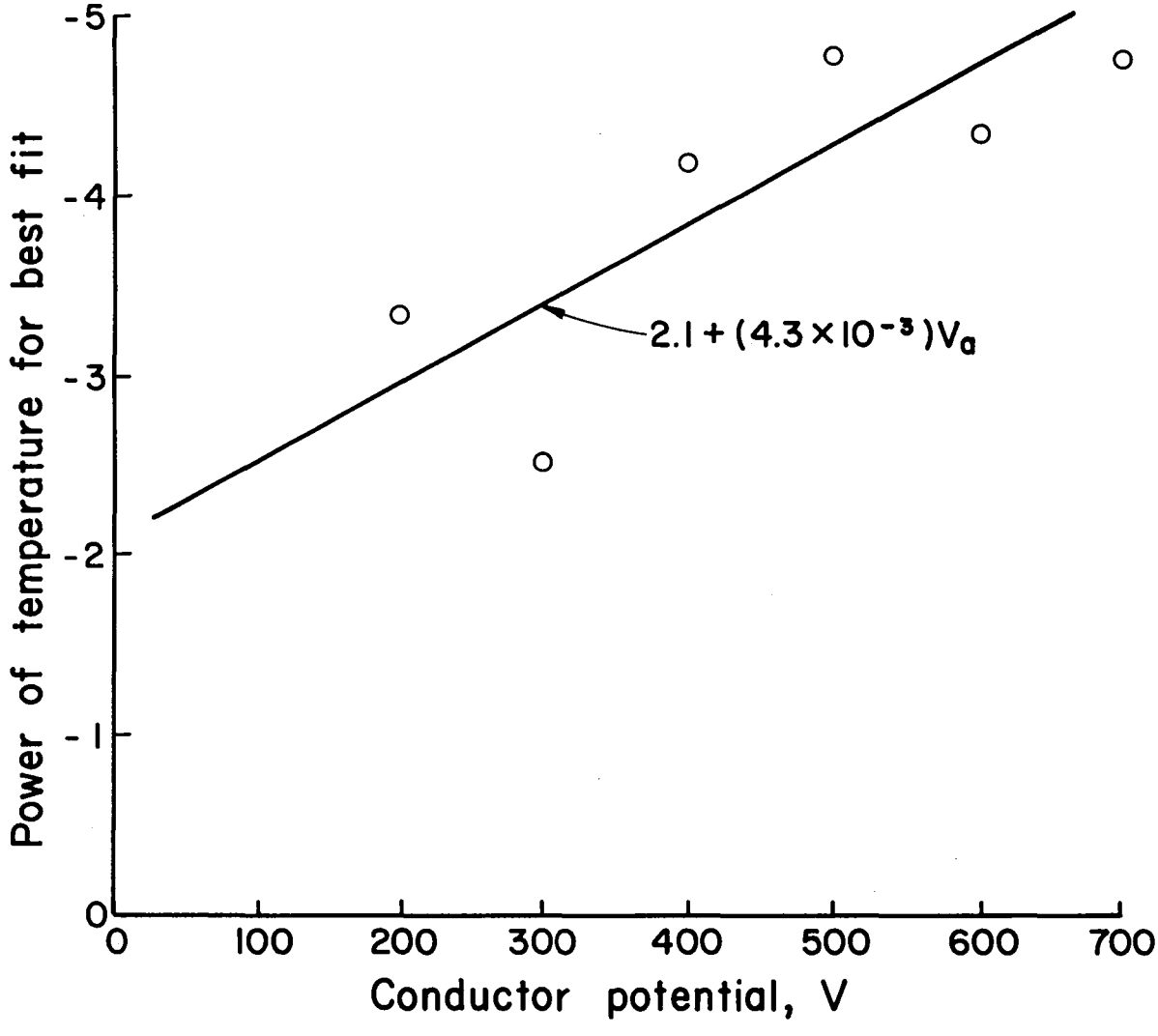


Fig. 4-2. Power of temperature variation for electron current as a function of conductor potential.

The expression for the current (Eq. 4-1) was then matched to 14 sets of data and the radius of insulator that contributes to collection was determined. The insulator radius is defined as

$$r_i \equiv r_c - r_h \ . \tag{4-4}$$

$r_i$ was assumed to be a function of only conductor potential for simplicity. The calculated values of the radius, $r_i$, were then fitted to a simple parabolic variation with potential. The best least-squares fit was obtained with (see Fig. 4-3)

$$r_i = 3.46 \times 10^{-8} \ V_a^{\ 2} \ . \tag{4-5}$$

In the model described in the previous section, there is a potential gradient along the surface of the collection area. This would imply that the potential in the term $\{1 + b^2/4 + (1 - b^2/4)\ eV/kT_e\}$ should be replaced by a potential averaged over the collection area. This could reduce this term, by as much as a factor of 3, which would mean that $r_i$ would have to be increased as much as by a factor of 1.7. Even with these considerations, these calculations still demonstrate that the model is feasible since the collection area, in the worst case, is only 50% of the sample size.

This empirical fit was then used to calculate expected current/voltage curves. Typical calculated curves are shown in Figs. 4-4 and 4-5, together with the corresponding experimental data. The empirical fit is shown to give reasonable agreement to experimental results in these comparisons, and can be used to give an order of

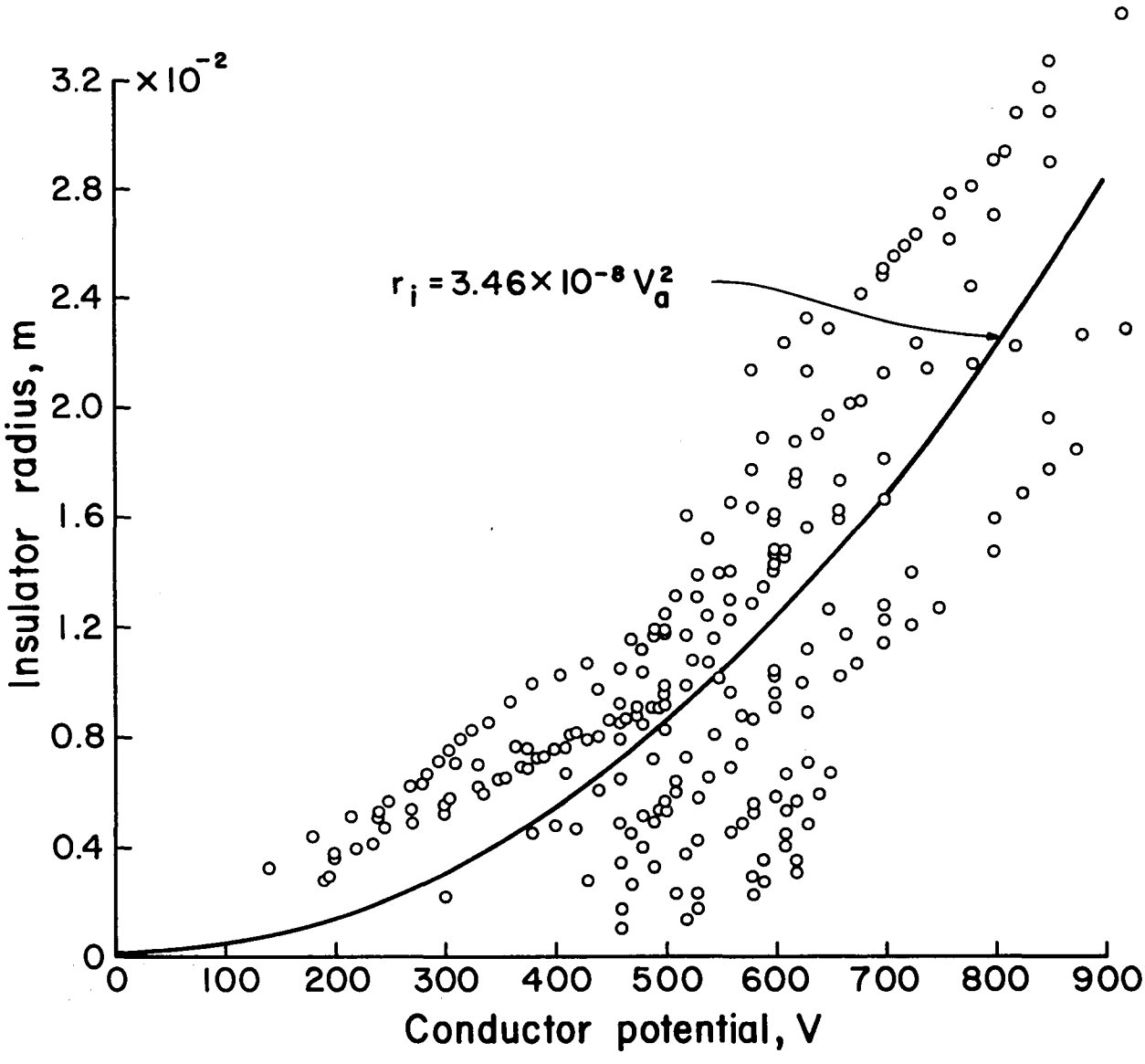


Fig. 4-3. Insulator collection radius as a function of conductor potential.

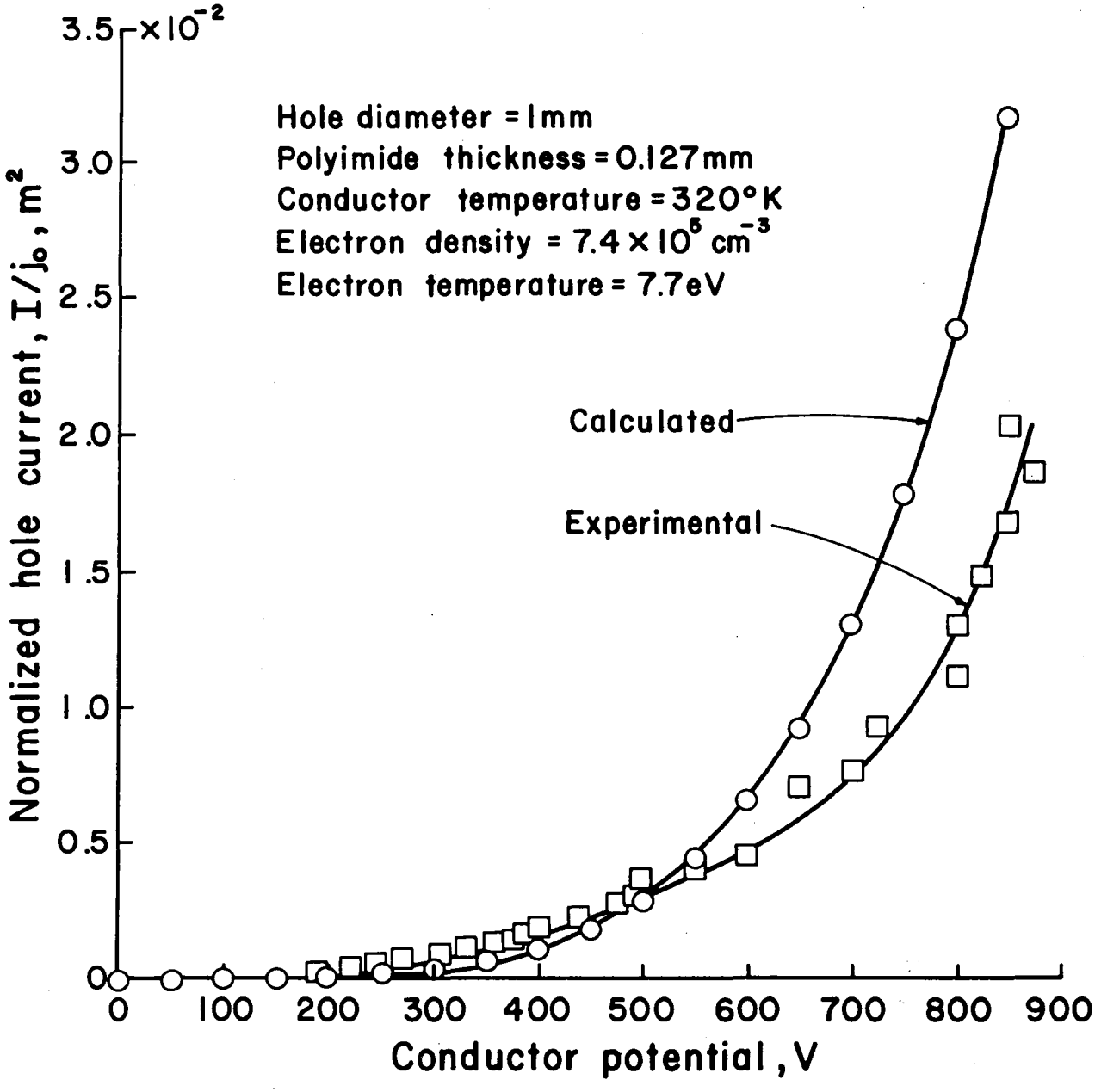


Fig. 4-4. Comparison of experimental and calculated electron current collection characteristics for a hole diameter of 1 mm, electron density of $7.4 \times 10^5$ $cm^{-3}$, electron temperature of 7.7 eV and conductor temperature of 320°K.

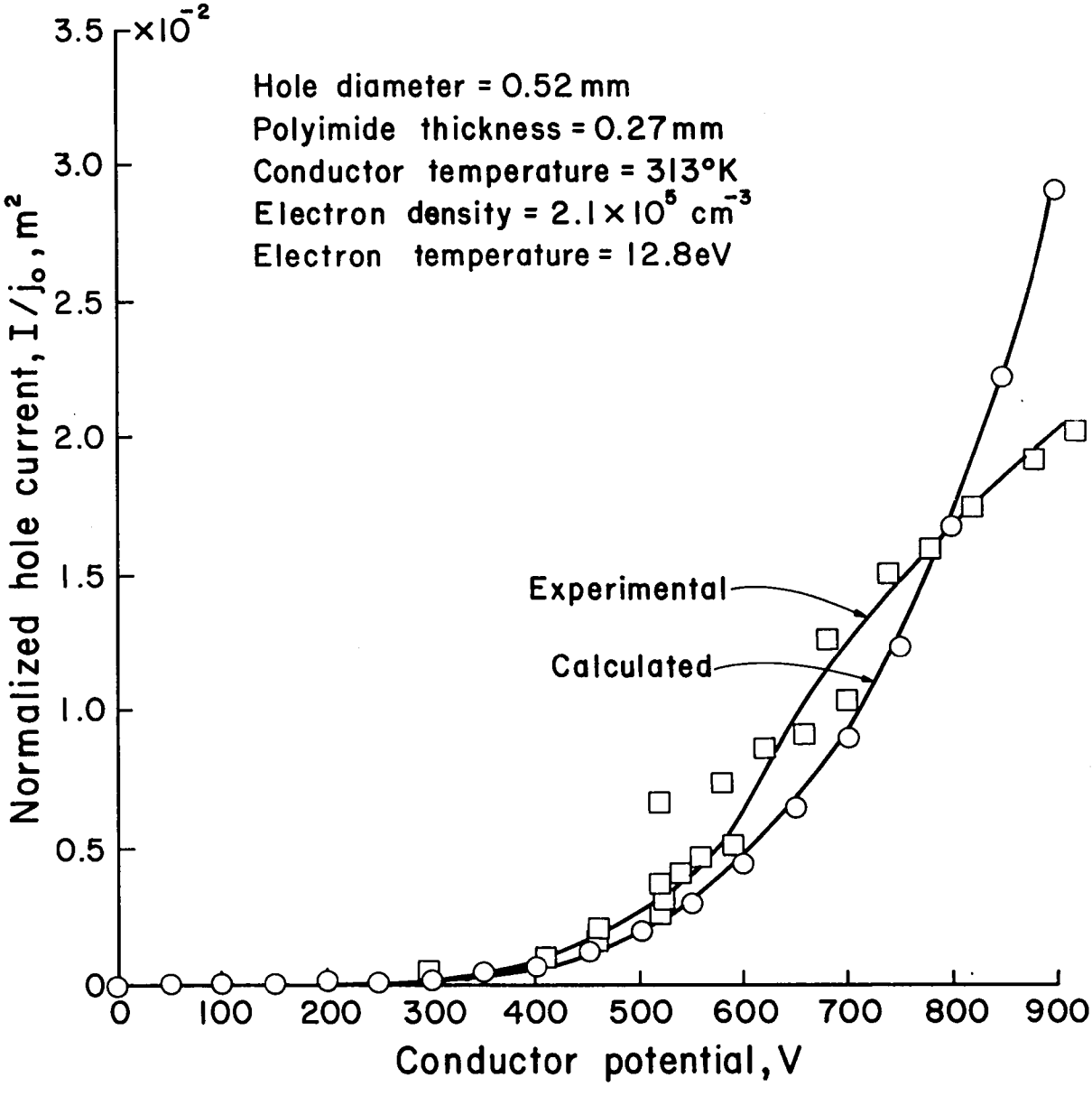


Fig. 4-5. Comparison of experimental and calculated electron current collection characteristics for a hole diameter of 0.52 mm, electron density of $2.1 \times 10^5$ $cm^{-3}$, electron temperature of 12.8 eV and conductor temperature of 313°K.

magnitude calculation or better of expected results. Because of the empirical fit used, a change in insulator material would require additional experimental data.

## Electron Trajectories Across the Insulator Surface

Further calculations were done to determine if the electron motion across the insulator surface (described earlier) were possible. To accomplish this, equations of motion for the electron moving across the insulator surface were needed. In the derivations of these equations, cylindrical coordinates (r, θ, z) are used. The radius along the surface of the insulator is r and z is the height above the surface of the sample.

Surface Charge Density. The first step is to derive an expression for the surface charge density. It is assumed that a constant current density, j in amps/$m^2$, is striking the collection area, $\pi r_c^2$. It is further assumed that the collection radius is a function of the applied conductor potential only. In the model, all electrons striking within the radius $r_c$ will be collected, so that a line current density, $j_L$ in amps/m, can be calculated for a specific radius, r.

$$j_L = \frac{\int_0^{2\pi} d\theta \int_r^{r_c} j\ r dr}{2\pi r} = \frac{j[r_c^2 - r^2]}{2r} \tag{4-6}$$

The surface charge density is then given by the expression

$$\sigma(r) = j_L/v_s \tag{4-7}$$

where $v_s$ is a surface velocity dependent only on the applied conductor potential. Thus

$$\sigma(r) = \frac{j}{2v_s}\frac{1}{r}(r_c^{\,2}-r^2) \ . \tag{4-8}$$

By introducing a dimensionless quality, $R \equiv r/r_c$, the normalized radius, the surface charge density takes the form

$$\sigma(R) = \frac{j}{2v_s} r_c \frac{1}{R}[1-R^2] \tag{4-9}$$

in which the term $jr_c/2v_s$ is a geometric factor dependent on the applied conductor potential and current density, j. In this form, a normalized surface charge density, $2v_s/jr_c\ \sigma(R)$ can be plotted against normalized radius, R, to give a profile that is independent of current density or applied conductor potential (see Fig. 4-6).

Surface Potential. With an expression for the surface charge density, a surface potential can be calculated across the radius $r_c$. The sample potential is given by the expression[5]

$$V(r) = \frac{1}{4\pi\varepsilon_o}\int_o^{2\pi} d\theta' \int_{r_h}^{r_c} \frac{\sigma(r')r'dr'}{[r^2+r'^2-2rr'\cos\theta']^{1/2}} \ . \tag{4-10}$$

where $\varepsilon_o$ is the permittivity of free space.

In terms of the normalized radius, the expression becomes

$$V(R) = \frac{jr_c^{\,2}}{8\pi\varepsilon_o v_s}\int_o^{2\pi} d\theta' \int_{R_h}^{1} \frac{(1-R'^2)dR'}{[R^2+R'^2-2RR'\cos\theta']^{1/2}} \tag{4-11}$$

where $R' \equiv r'/r_c$ and $R_h = r_h/r_c$. From this a normalized potential, $8\pi\varepsilon_o v_s/jr_c^{\,2}\ V(R)$, can be calculated. This was desirable since the integral (Eq. 4-11) could not be solved analytically, the numerical solution (see Fig. 4-7) would be independent of conductor potential

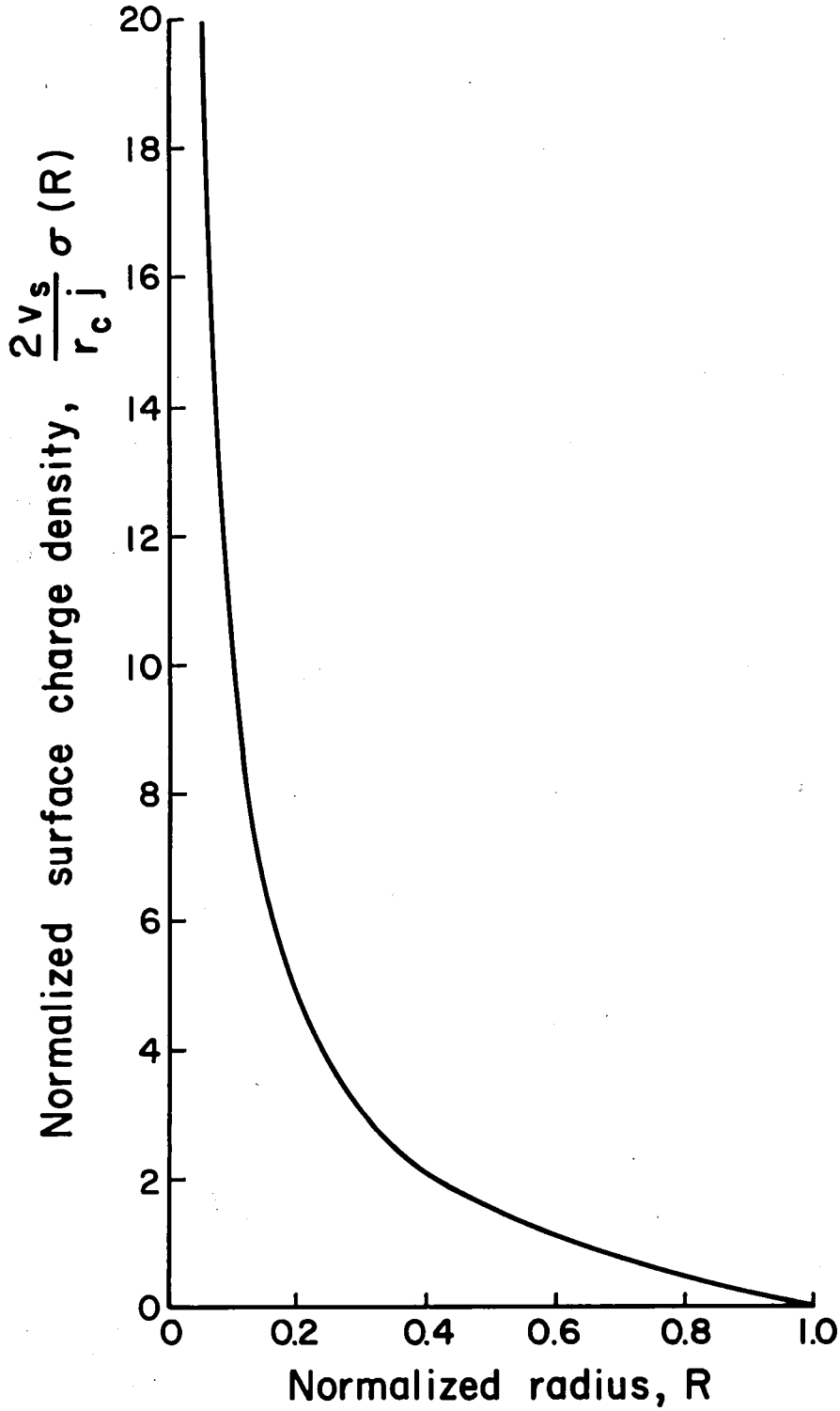


Fig. 4-6. Normalized surface charge density as a function of normalized radius.

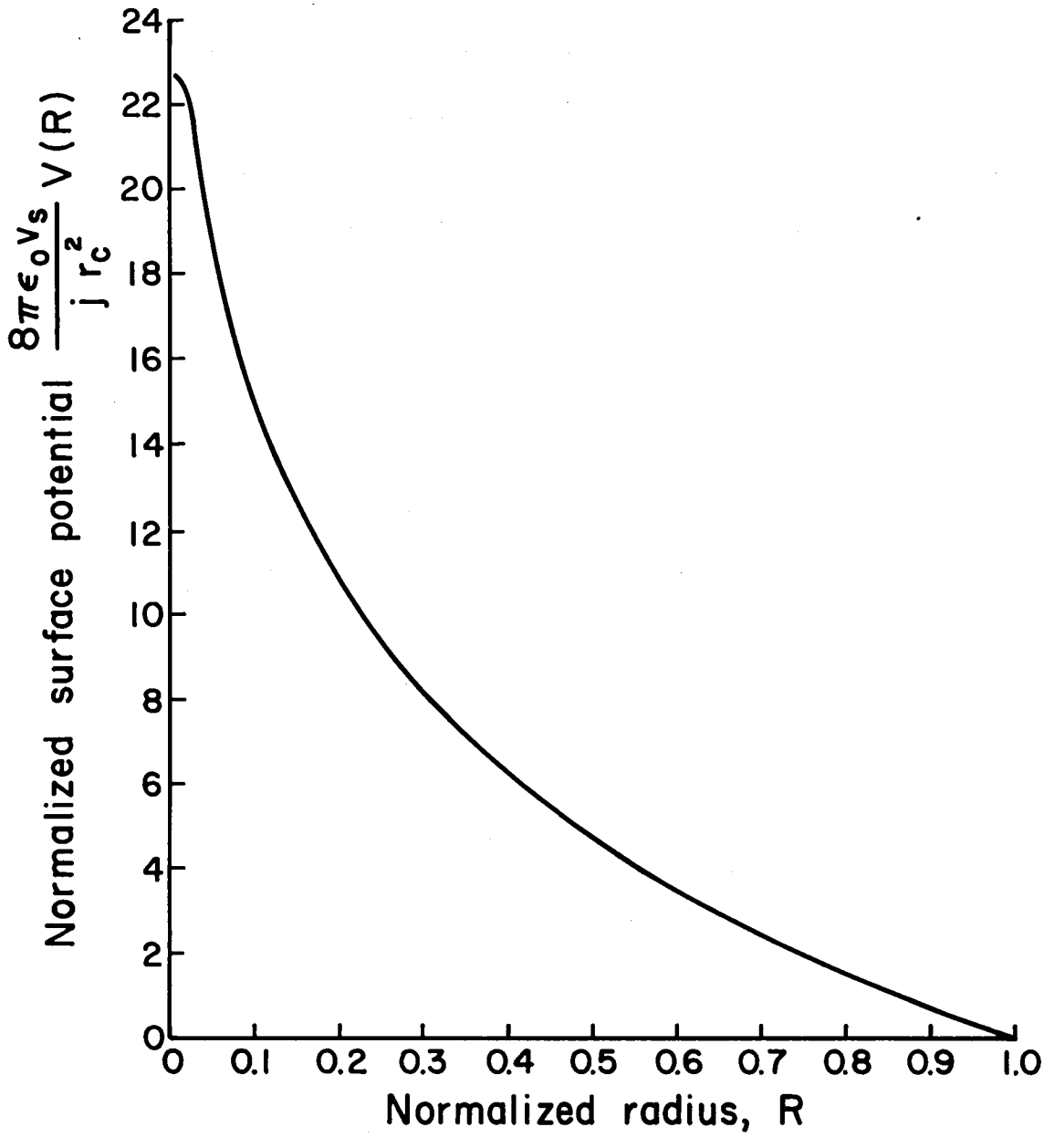


Fig. 4-7. Normalized surface potential as a function of normalized radius.

or current density. The numerical solution is shown as a function of normalized radius.

To get estimates of the values of j and $r_c$, as a function of applied conductor potential, the equations developed in the previous section (collection area) for the current (Eq. 4-1) and the empirical expression for $r_i$ (Eq. 4-5) were used. The approximation $r_i \approx r_c$, was used to estimate $r_c$ (the approximation is reasonable inasmuch as $r_h << r_i$). The current density was found using

$$I = j\pi r_c^2 \ . \tag{4-11}$$

The calculated value for the current was used rather than actual data because the expression for the current (Eq. 4-1) is representative of a large set of data.

Once the values of j and $r_c$ were known, $v_s$ was calculated by

$$v_s = \frac{j\pi r_c^2}{8\pi\varepsilon_o}\left[\frac{V(R_h)-V(1)}{V_a}\right]$$

or (4-12)

$$v_s = \frac{I}{8\pi^2\varepsilon_o}\,\frac{V(R_h)-V(1)}{V_a} \ .$$

These values are tabulated for the case in which the hole radius is 0.5 mm, electron temperature is 7.7 eV, electron density is $7.4 \times 10^5/cm^3$, and conductor temperature is 320°K (see Table 4-1).

<u>Electric Field Along the Surface</u>. The normalized surface potential was approximated by the curve

Table 4-1. Collection Radius, Collected Current, Current Density, Surface Velocity and Normalized Hole Radius for Various Values of Conductor Potential.

| Conductor Potential (volts) | Collection Radius (m) | Collected Current (amps) | Current Density (amps/$m^2$) | Surface Velocity (m/sec) | Normalized Hole Radius ($r_h/r_c$) |
|---|---|---|---|---|---|
| 300 | $3.11\times10^{-3}$ | $1.21\times10^{-5}$ | 0.398 | $7.00\times10^{2}$ | 0.161 |
| 350 | $4.24\times10^{-3}$ | $2.52\times10^{-5}$ | 0.446 | $1.43\times10^{3}$ | 0.118 |
| 380 | $5.00\times10^{-3}$ | $3.74\times10^{-5}$ | 0.476 | $2.11\times10^{3}$ | 0.100 |
| 400 | $5.54\times10^{-3}$ | $4.74\times10^{-5}$ | 0.492 | $2.64\times10^{3}$ | 0.090 |
| 425 | $6.25\times10^{-3}$ | $6.33\times10^{-5}$ | 0.516 | $3.45\times10^{3}$ | 0.080 |
| 454 | $7.14\times10^{-3}$ | $8.65\times10^{-5}$ | 0.540 | $4.61\times10^{3}$ | 0.070 |
| 491 | $8.33\times10^{-3}$ | $1.26\times10^{-4}$ | 0.578 | $6.51\times10^{3}$ | 0.060 |
| 538 | $1.00\times10^{-2}$ | $1.91\times10^{-4}$ | 0.608 | $9.48\times10^{3}$ | 0.050 |
| 601 | $1.25\times10^{-2}$ | $3.23\times10^{-4}$ | 0.658 | $1.52\times10^{4}$ | 0.040 |
| 650 | $1.46\times10^{-2}$ | $4.63\times10^{-4}$ | 0.691 | $2.09\times10^{4}$ | 0.034 |
| 695 | $1.67\times10^{-2}$ | $6.36\times10^{-4}$ | 0.726 | $2.74\times10^{4}$ | 0.030 |
| 750 | $1.95\times10^{-2}$ | $9.11\times10^{-4}$ | 0.763 | $3.74\times10^{4}$ | 0.026 |
| 800 | $2.21\times10^{-2}$ | $1.22\times10^{-3}$ | 0.795 | $4.81\times10^{4}$ | 0.023 |
| 850 | $2.50\times10^{-2}$ | $1.61\times10^{-3}$ | 0.819 | $6.06\times10^{4}$ | 0.020 |

$$\frac{8\pi\varepsilon_o v_s}{jr_c^2} V(R) \approx \frac{6.263}{R^{1/2}} - \frac{0.038}{R^{3/2}} - 4.665 \ . \tag{4-13}$$

The electric field along the surface could then be found by[5]

$$E_r(r) = \frac{\partial V(r)}{\partial r} \ . \tag{4-14}$$

This yielded, in terms of normalized radius

$$E_r(R) = \frac{jr_c}{8\pi\varepsilon_o v_s} \left[ \frac{3.131}{R^{3/2}} - \frac{0.0564}{R^{5/2}} \right] . \tag{4-15}$$

A plot of the normalized electric field along the surface, $8\pi\varepsilon_o v_s/jr_c \ E_r(R)$ versus normalized radius is shown in Fig. 4-8.

Sample Calculations. The surface charge density, surface potential and electric field along the surface were calculated as a function of normalized radius for an applied conductor potential of 601 volts. This was done to illustrate the magnitude of these quantities. The equations of motion that will be solved will be for this condition. The quantities are plotted in Fig. 4-9.

Electric Field Above the Surface. To write the equations of motion, it is necessary to estimate the electric field above the surface of the sample. Two approaches are possible. One, that the electrons traversing the surface are influenced only by the local surface charge density. In this case, the electric field, $E_z$, may be approximated by[5]

$$E_z = \sigma/\varepsilon_o \ . \tag{5-16}$$

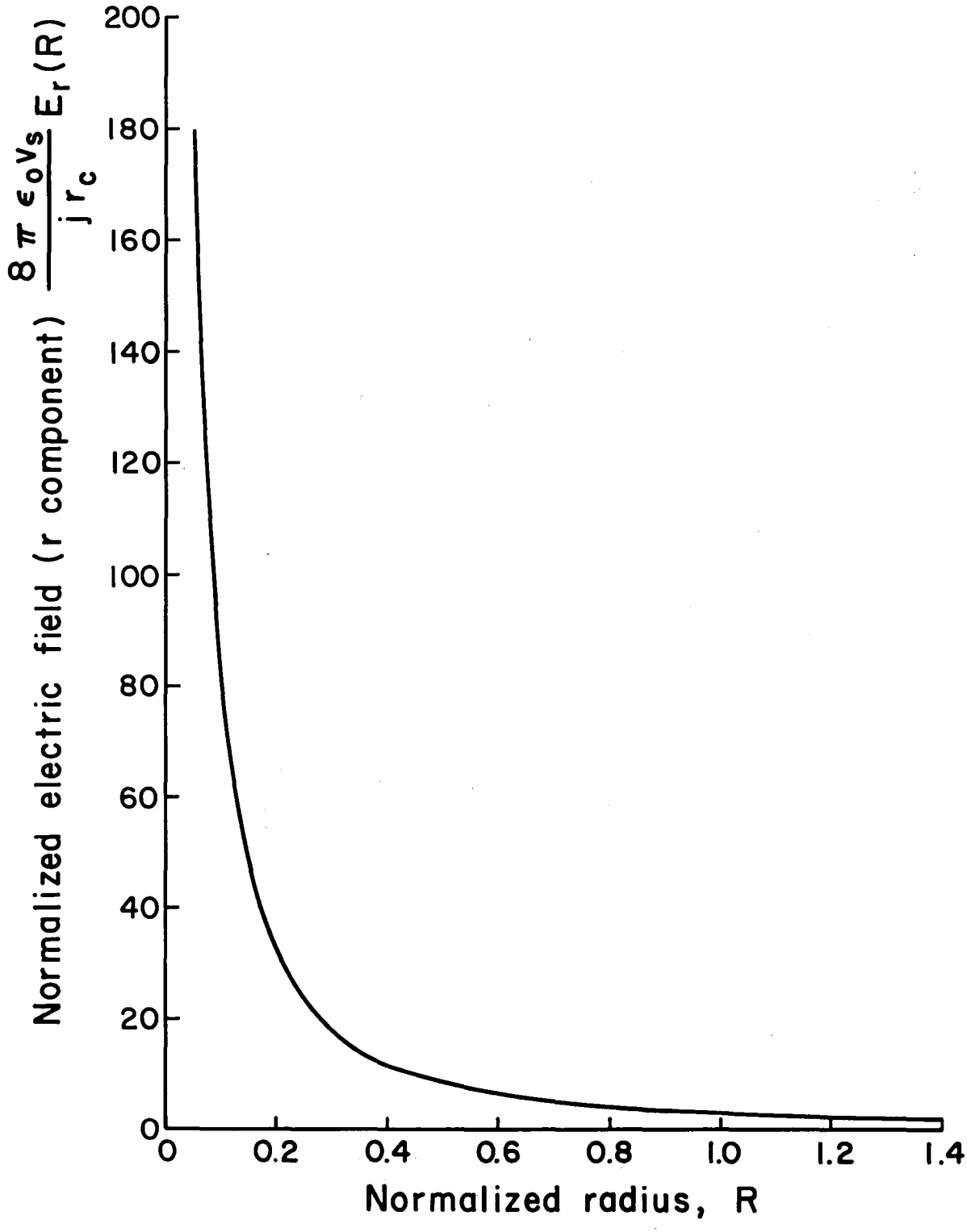


Fig. 4-8. Normalized electric field along the surface as a function of normalized radius.

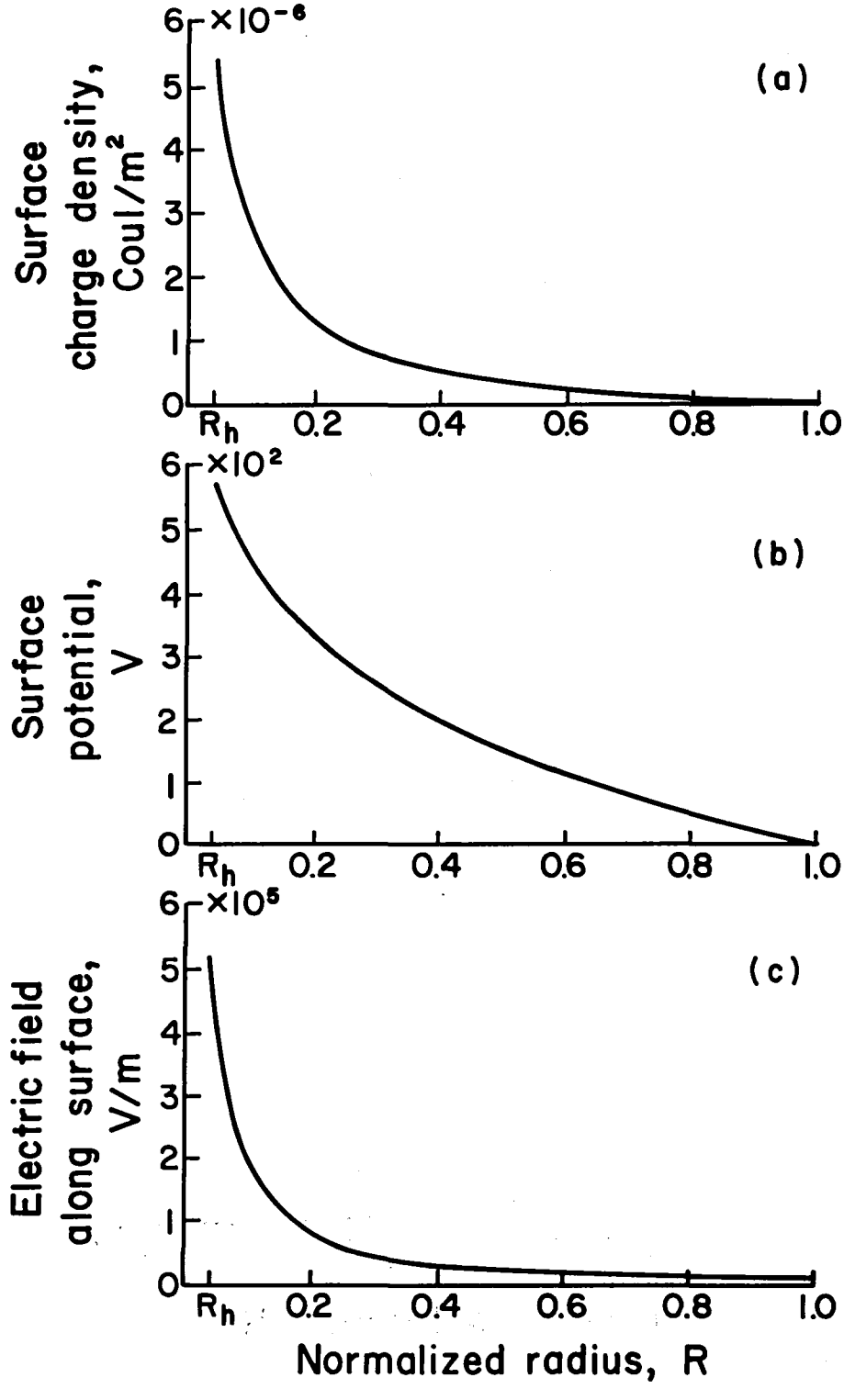


Fig. 4-9. The (a) surface charge density, (b) surface potential, and (c) electric field along the surface plotted against normalized radius for an applied conductor potential of 601 volts.

The alternate approach is that the electrons moving across the surface are affected by the sheath between the surface and the plasma. In this case, the potential is approximated by Child's law[6]

$$\phi(z_{max} - z) = \left(\frac{9j}{4\varepsilon_o}\right)^{2/3} \left(\frac{m_e}{2e}\right)^{1/3} (z_{max} - z)^{4/3} \tag{4-17}$$

or

$$\tilde{\phi}(z) = \left\{ V(R)^{3/4} - \left(\frac{9j}{4}\right)^{1/2} \left(\frac{m_e}{2e}\right)^{1/4} z \right\}^{4/3} \tag{4-18}$$

where z is zero on the surface of the insulator and $z = z_{max}$ at $\phi = 0$, and V(R) is given by Eq. (4-13). The electric field for Child's law is then

$$E_Z(r,z) = \frac{4}{3} \left(\frac{9j}{4\varepsilon_o}\right)^{1/2} \left(\frac{m_e}{2e}\right)^{1/4} \left\{ V(R)^{3/4} - \left(\frac{9j}{4\varepsilon_o}\right)^{1/2} \left(\frac{m_e}{2e}\right)^{1/4} z \right\}^{1/3}. \tag{4-19}$$

Both these fields are plotted as a function of normalized radius for a conductor potential of 601 volts on Fig. 4-10 (Child's law electric field for z = 0). The electric fields differ by two orders of magnitude and should yield very different trajectories for the electrons crossing the insulator surface. It should then be possible to choose the correct approach to the z component of the electric field after examining the trajectories that each approach yields.

<u>Equations of Motion</u>. The equation of motion for r is given by

$$\frac{d^2r}{dt^2} = \frac{-eE_r}{m_e} = \frac{-ejr_c}{8\pi\varepsilon_o m_e v_s} \left[ \frac{3.131}{(r/r_c)^{3/2}} - \frac{0.0564}{(r/r_c)^{5/2}} \right] . \tag{4-20}$$

Introducing the dimensionless time variable

$$\tau \equiv \sqrt{\frac{je}{8\pi\varepsilon_o m_e v_o}} \; t \tag{4-21}$$

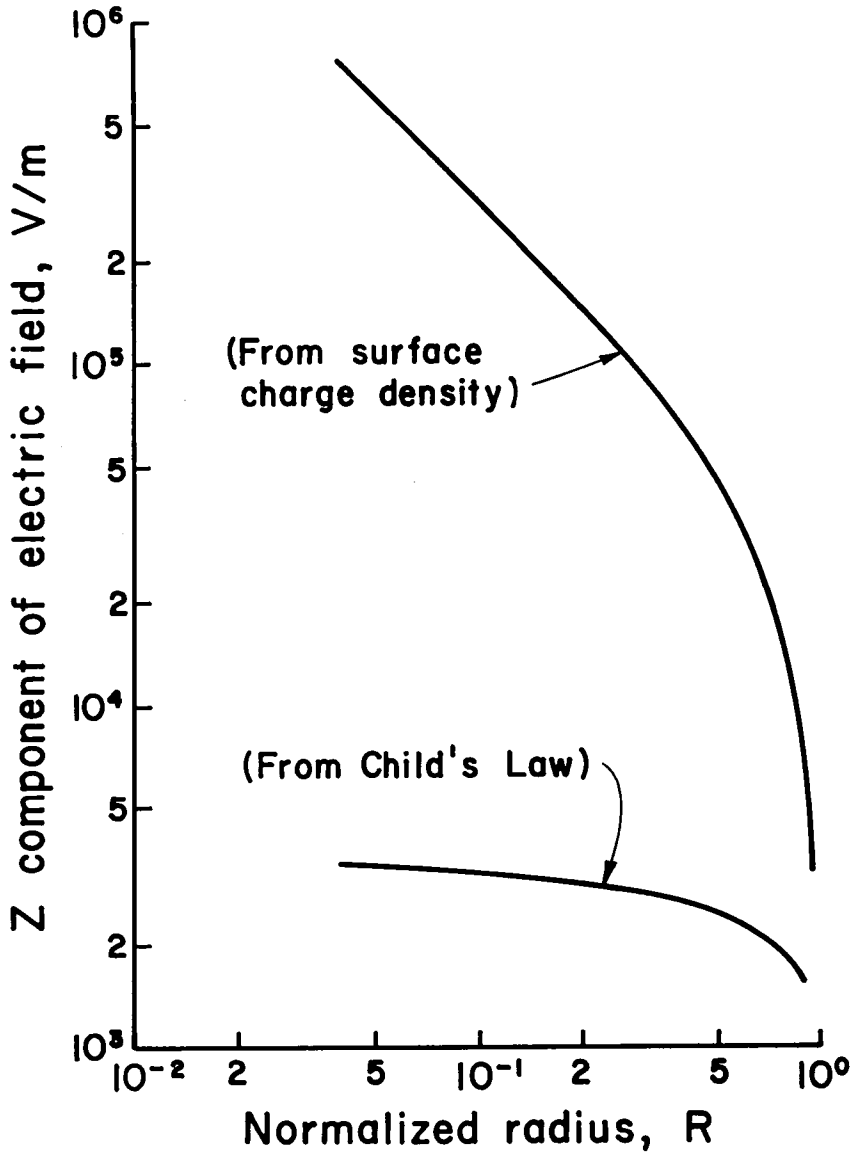


Fig. 4-10. Two possible electric fields above the surface as a function of normalized radius for conductor potential of 601 volts.

and the normalized radius, R, the equation of motion for r becomes

$$\frac{d^2R}{d\tau^2} = \left[\frac{3.131}{R^{3/2}} - \frac{0.0564}{R^{5/2}}\right] \quad . \tag{4-22}$$

For the equation of motion for z

$$\frac{d^2z}{dt^2} = \frac{-eE_z}{m_e} \quad . \tag{4-23}$$

The surface charge density electric field yields

$$\frac{d^2z}{dt^2} = \frac{-ej}{2v_s\varepsilon_o m_e} \frac{r_c^{\,2}}{r}\left[1 - \left(\frac{r}{r_c}\right)^2\right] \quad . \tag{4-24}$$

Introducing the dimensionless variable

$$Z \equiv \frac{z}{r_c} \tag{4-25}$$

the equation of motion, in dimensionless form, becomes

$$\frac{d^2Z}{d\tau^2} = -4\pi \frac{1}{R}\left(1 - R^2\right) \quad . \tag{4-26}$$

The Child's law electric field gives

$$\frac{d^2Z}{d\tau^2} = -\frac{32\pi\varepsilon_o v_s}{3jr_c}\left(\frac{9j}{4\varepsilon_o}\right)^{1/2}\left(\frac{m_e}{2e}\right)^{1/4}\left[V(R)^{3/4} - \left(\frac{9j}{4\varepsilon_o}\right)^{1/2}\left(\frac{m_e}{2e}\right)^{1/4} r_c z\right]^{1/3} \tag{4-27}$$

There are two sets of two coupled second order differential equations to be solved. They were solved numerically using a Runge-Kutta fifth order method for a system of first order coupled differential equations. This was done by introducing the variables

$$\zeta \equiv \frac{dR}{d\tau} \tag{4-28}$$

$$\xi \equiv \frac{dZ}{d\tau} \tag{4-29}$$

which correspond to dimensionless velocities in the r and z directions, respectively. The conditions solved for were for a conductor potential of 601 volts, an initial position on the surface of the insulator at the collection radius, $r_c$, and an initial velocity in the z direction equivalent to 2 eV. These conditions are for an electron striking the insulator at $r = r_c$ and emitting a secondary electron normal to the surface. An energy of 2 eV was picked to correspond to the probable energy of a secondary electron (see Appendix B).

The trajectories given by the differential equations are shown in Fig. 4-11. For $E_z$ calculated from the surface charge density, the trajectory took 44 hops across the insulator, with all the hops, after the initial hop, gaining, from the potential gradient across the surface, approximately 10 eV or less. These conditions would not permit the proposed secondary electron emission mechanism to take place.

The trajectory yielded by the Child's law approach to $E_z$ is more consistent with the proposed model. The energy gained by the first hop was approximately 60 eV, and for any initial position for $R < 1$, no more than two hops were ever necessary to reach the hole (from further calculations, not shown). By examining the electric fields, the condition necessary for trajectories feasible with the proposed model is

$$E_r \gg E_z \quad .$$

Calculating the Child's law sheath thickness, the sheath would appear to be a large spike on the surface of the insulator. This sheath is many

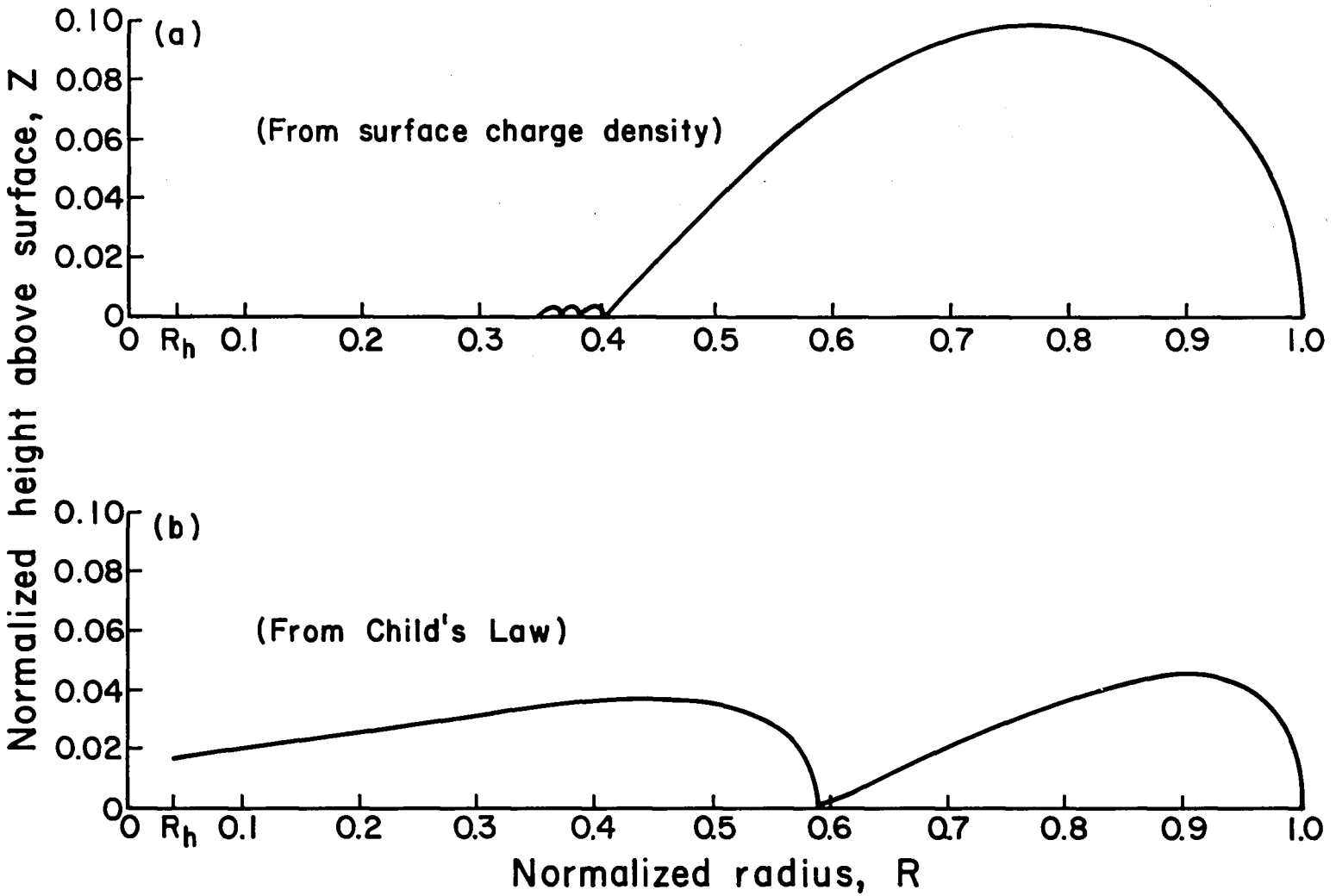


Fig. 4-11. Electron trajectories for an electron moving across the insulator for $E_z$ calculated from (a) the surface charge density and (b) Child's law, for a conductor potential of 601 volts and initial velocity equivalent to 2 eV normal to the surface.

times the collection radius (see Fig. 4-12, $Z_{max} \equiv z_{max}/r_c$). This is in contradiction to the proposed model. The sheath is unphysical and fails to provide a uniform current density to the collection area.

These calculations show that the proposed approach has been incorrect in assuming that the collection area is large. The two possible solutions within the framework of the model contradict it. The local charge density solution has the correct sheath (planar), but the trajectories are inconsistent with the secondary electron mechanism of surface conduction. The Child's law solution has the correct trajectory but the sheath is unphysical. This says that the correct trajectories cannot be obtained with a planar type sheath. The alternative to this is a large sheath surrounding a small collection area (see Fig. 4-13). A spherical sheath much larger than the collection area would allow the condition for the correct trajectories, $E_r >> E_z$, to take on the much reduced collection area.

The conclusion of this analysis, then, is that the sheath should be approximately hemispherical. The radius for secondary electron emission (collection radius) is much smaller than the sheath radius. Between the collection radius and the sheath radius, the electron trajectories should be nearly radial to avoid collisions with the insulator surface and a resultant buildup of charge on that surface. Between the collection radius and hole radius, surface conduction takes place with the secondary electron mechanism. This approximate model will be studied and tested in future work.

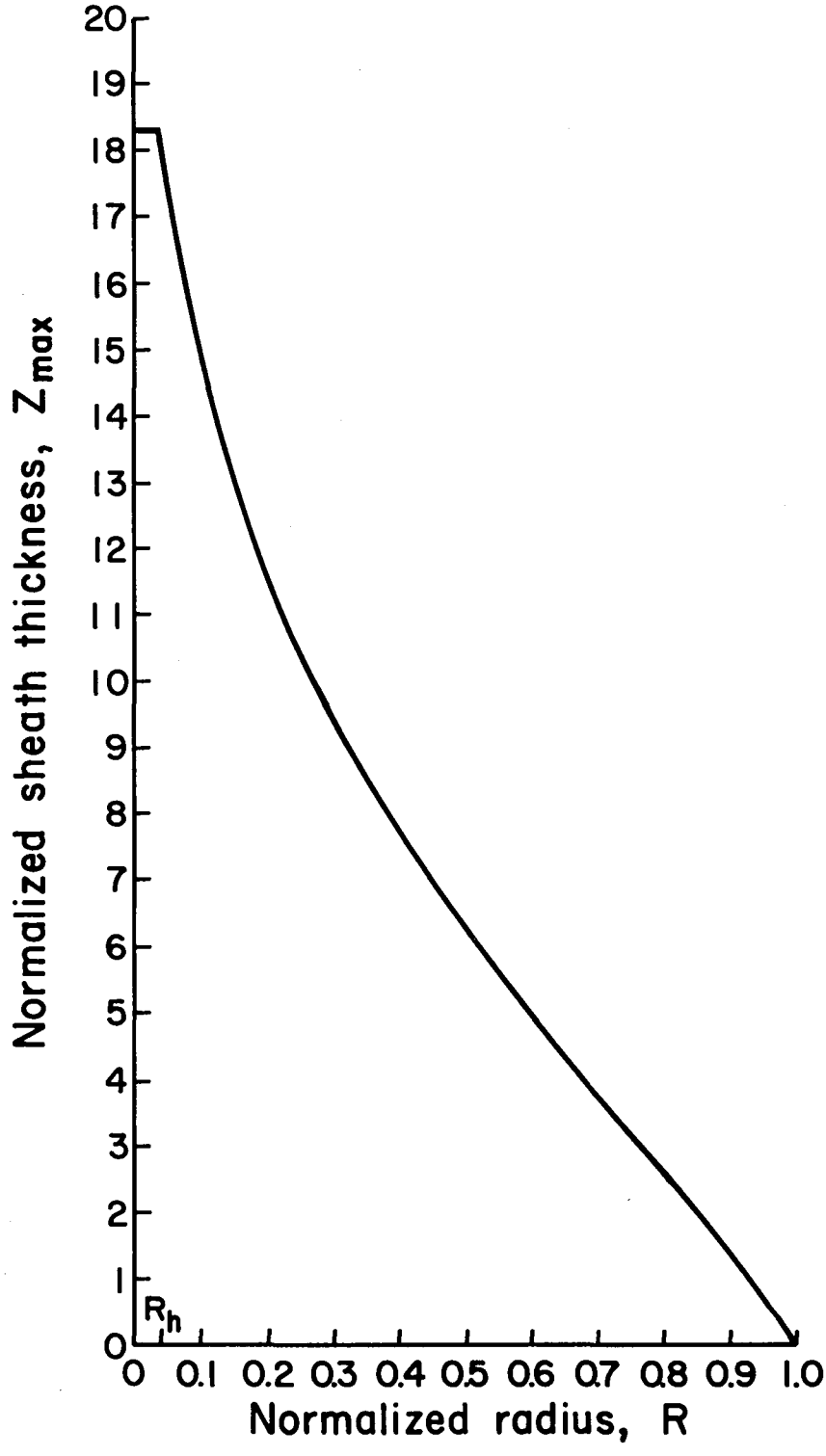


Fig. 4-12. Normalized sheath thickness, for Child's law sheath, as a function of normalized radius for a conductor potential of 601 volts.

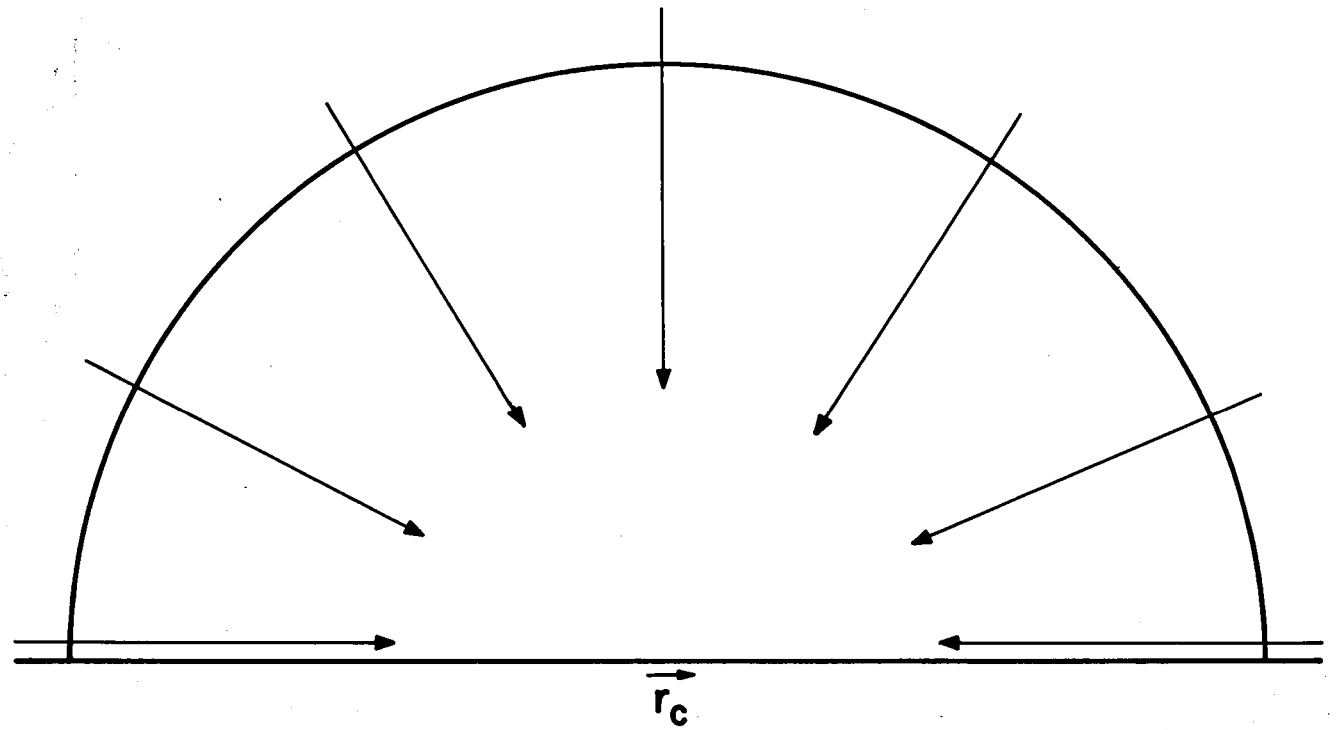


Fig. 4-13. Schematic of proposed model with hemispherical sheath.

## V. CONCLUDING REMARKS

A glow discharge electron collection mode appears at high currents (>1.5 mA). This collection mode appears to be related to the background neutral density and as such does not simulate a process that would occur in a space environment. Data taken before this mode change occurs are in rough agreement with an earlier investigation,[1] indicating that most of the tests taken to date are still valid for space simulation. Future tests should be done in an environment that has a lower neutral density than is presently used. Data indicate a density below $3 \times 10^{12}$ $cm^{-3}$ should be adequate to avoid the glow discharge mode with argon.

Negative bias (ion collection) tests indicate that electrostatic collection occurs for low voltages (<-1000 volts) but another mechanism occurs at high voltages. This other mechanism results in a brownish film being deposited on the exposed conductor area, decreasing ion current collection. The deposited film suggests that sputtering or vaporization of the polyimide is taking place. The tests in the high voltage regime exhibited oscillation of current and voltage, indicating that a regulated power supply should be used in future experiments.

The modeling of electron collection was attempted. The model assumed a large collection region over the insulator with a sheath covering approximately the same area. Calculations show the model to be inconsistent with the assumptions, indicating that a model with a small collection region and a large hemispherical sheath should be considered.

APPENDIX A

# AIAA-81-0741
# Experimental Simulation of Space Plasma Interactions with High Voltage Solar Arrays

R.P. Stillwell, H.R. Kaufman and R.S. Robinson, Colorado State University, Fort Collins, Colo.

50th Anniversary 1981

**AIAA/JSASS/DGLR 15th International Electric Propulsion Conference**

April 21-23, 1981 / Las Vegas, Nevada

For permission to copy or republish, contact the American Institute of Aeronautics and Astronautics • 1290 Avenue of the Americas, New York, N.Y. 10104

# EXPERIMENTAL SIMULATION OF SPACE PLASMA INTERACTIONS WITH HIGH VOLTAGE SOLAR ARRAYS

R. P. Stillwell, H. R. Kaufman, and R. S. Robinson
Colorado State University
Fort Collins, Colorado 80523

## Abstract

Operating high voltage solar arrays in the space environment can result in anomalously large currents being collected through small insulation defects. Tests of simulated defects have been conducted in a 45 cm vacuum chamber with plasma densities of $10^5$ to $10^6$ $cm^{-3}$. Plasmas were generated using an argon hollow cathode. The solar array elements were simulated by placing a thin sheet of polyimide (Kapton) insulation with a small hole in it over a conductor. Parameters tested were: hole size, adhesive, surface roughening, sample temperature, insulator thickness, insulator area. These results are discussed along with some preliminary empirical correlations.

## Introduction

Solar cell arrays constitute the major source of reliable long-term power for spacecraft orbiting the earth. High voltage arrays are desired to optimize both spacecraft mass and power efficiency. The space plasma environment, though, can result in large currents being collected by exposed solar cells, with corresponding reductions in power output from the array. The obvious solution of using a covering of transparent insulation is at least partially offset by the expectation of defects, either from the manufacturing process or resulting from collisions with micrometeors. Early experiments showed that positive electrodes behind pinhole openings in the insulating sheets could collect electron currents far in excess of what would be expected from electrostatic theory.[1-5] At high enough plasma densities and electron currents, the current collection process degrades into a visible arc. At low plasma densities, the large electron currents are collected in the absence of a visible arc, and appear to be associated with an essentially nondestructive surface phenomenon. The maximum current at high voltage appears, from previous investigations, to depend primarily on the plasma density and the area of the insulating surface surrounding the pinhole. The major emphasis of this research is the understanding of the apparent surface conduction by which the area of insulation surrounding an exposed conductor enhances the current collection. Experimental tests of high voltage current collection simulating both insulator defects and plasma environments are described.

## Apparatus and Procedure

All tests were conducted in a 45 cm diameter, 45 cm long cylindrical vacuum system. An argon hollow cathode mounted horizontally at the base of the vacuum system was used as the source of the plasma. The hollow cathode supplied electrons which then ionized the argon. A protected array of solar cells was simulated by placing a sheet of insulating material over a conductor. The insulating sheet of polyimide (Kapton) was held to the conductor by a space-qualified adhesive, except for the few tests conducted to evaluate collection characteristics in the presence of lower quality adhesives. A small hole was punched or drilled into the insulating sheet to simulate the defect. The sample was mounted in the center of the vacuum system.

The operating pressure in the vacuum system was in the range of $9\text{-}30 \times 10^{-5}$ Torr. The plasma density ranged from $1\text{-}25 \times 10^5$ $cm^{-3}$. This plasma range approximates the environments expected for both an electrically propelled spacecraft, due to its own charge exchange plasma[6] and a spacecraft in a natural low earth orbit plasma environment.[7]

The procedure for making a test was to allow the sample to be bombarded by the plasma for at least one hour to stimulate desorption of gases on the insulator surface. The current collected through the hole was monitored as the potential on the conductor was increased.

## Results and Discussion

### Positive Bias

High Current Measurements. In collecting high currents, up to 5 mA, there appears to be a change in collection modes, indicated by the dashed line in Fig. 1. During tests a bluish glow was observed to increase in intensity and extent with the change in mode (toward increasing current). From these observations, a possible explanation for the mode change is a glow discharge initiation involving background neutrals. Because this glow discharge process is probably associated with the high background pressure (higher than in a space environment), most of the data presented herein will be at a current below any major mode change, unless otherwise indicated.

Pinhole Size. Four hole diameters were investigated: 0.35, 0.52, 1.0, and 2.0 mm. This range of diameters spanned an area range of over 30:1. To isolate the effect of the area of exposed conductor from plasma density effects, the current was normalized. The random electron current density in a plasma is given by[8]

$$j_o = en\left[\frac{kT_e}{2\pi m_e}\right]^{1/2} \qquad (1)$$

where e is the electronic charge, n is the electron density, k is Boltzmann's constant, $T_e$ is the electron temperature, and $m_e$ is the electron mass.

It would be expected that the current collected through a hole in an insulating sheet would vary with plasma density, proportional to the random electron current density given above. Another possible normalizing relationship considered is this current density times the area of the hole in the insulating sheet, $I_o = j_o A_{hole}$.

Released to AIAA to publish in all forms.

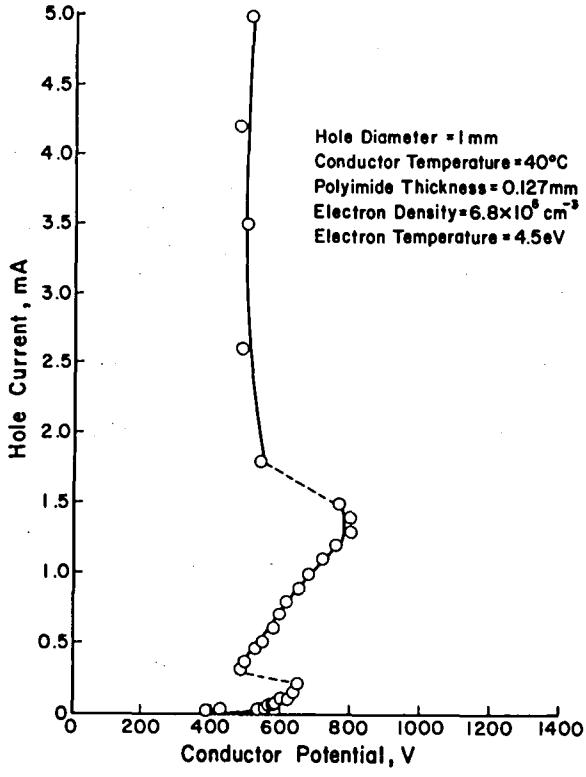


Fig. 1. Electron current collection characteristics extended to higher currents.

The data were normalized using both the random current density and the random current, see Fig. 2(a) and 2(b). The better correlation obtained with $j_o$ indicates that electron current collection at these densities is insensitive to hole area.

As seen in Fig. 2(a), anomalously low currents were initially collected with the large 2 mm hole; however, at higher collection currents, some mode change occurred that brought the data for this hole diameter more in agreement with the other data. This mode change was not associated with any visible glow discharge and was well below the other mode changes associated with high collection currents. It was also a repeatable phenomenon. At this point it can neither be explained nor ignored.

These results are not in agreement with those reported earlier by Kennerud,[5] who found an effect due to hole area; however, the magnitudes of the normalized current collection data are in rough agreement. The difference is possibly due to differences in experimental conditions. This investigation used an argon hollow cathode for a plasma source, had an electron density range of 1-25 × $10^5$ $cm^{-3}$ and a background pressure range of 9-30 × $10^{-5}$ Torr. The previous investigation used a directed ion beam composed of nitrogen for the plasma source, an electron density of 2-17 × $10^3$ $cm^{-3}$ and a background pressure range of 1-10 × $10^{-5}$ Torr.

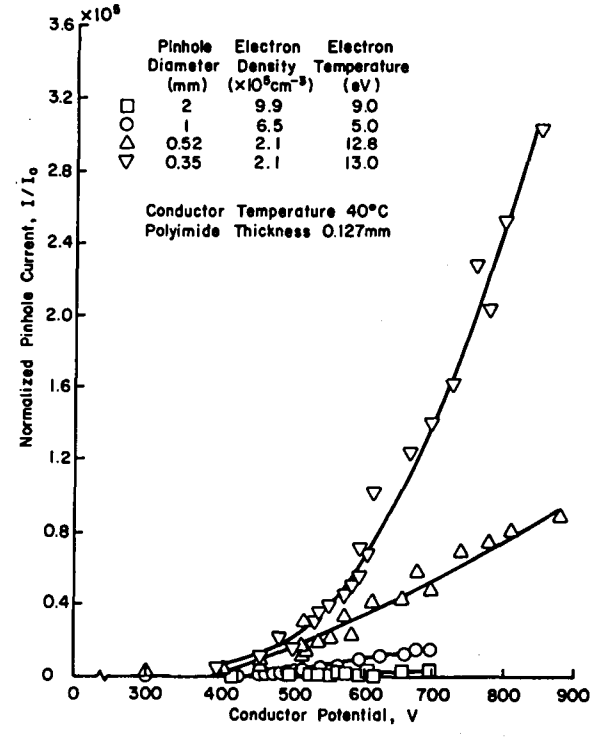


(a)

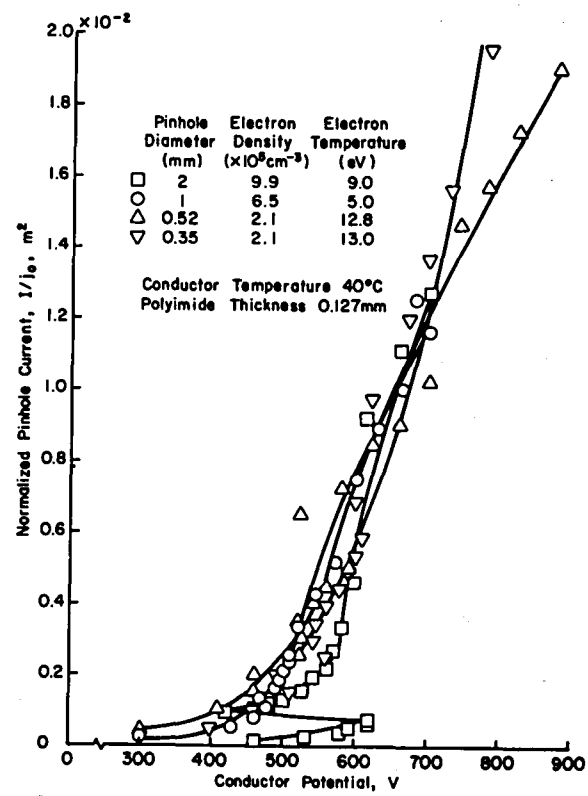


(b)

Fig. 2. Electron current collection characteristics for a range of hole sizes, normalized by (a) $I_o$, (b) $j_o$.

Adhesive. Although most of the tests were made with a space qualified adhesive (Y966, by 3M), some tests were also conducted using a low priced commercial brand (Scotch Double Stick, also by 3M). Tests were conducted at two temperatures, 27 and 95°C. The low priced commercial adhesive was found to have modified sticking properties (i.e., adhesive was soft and pliable) after testing at higher temperatures, while no such change was evident for the space qualified adhesive. Such a change in properties for an organic material in a vacuum environment is almost always associated with outgassing. This outgassing should be increased at the high temperature. Figure 3 shows the results of these tests. It can be seen from Fig. 3 that there appears to be no significant effect of the adhesive tests, hence probably no effect due to outgassing from the adhesive. Other tests without any adhesive tended to support this conclusion. Except for more data scatter, possibly due to varying the distance between adhesive and sample, the data with no adhesive agreed with Fig. 3.

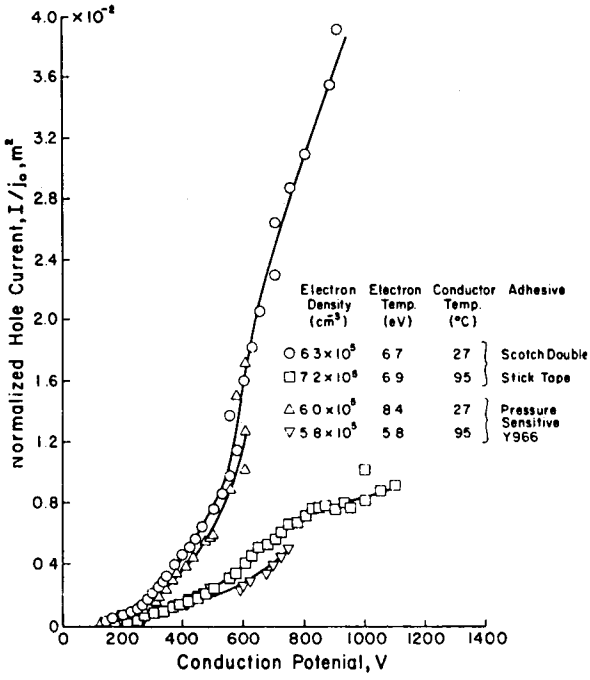


Fig. 3. Effect of adhesive type and sample temperature on electron collection.

Fresh and Old Samples. Subsequent tests made on the same sample exhibited a lack of reproducibility compared to the initial test on that sample. There was a general degradation in current collected with repeated tests, as shown in Fig. 4. One possible explanation for this effect was that adsorbed gas on the insulator surface was involved in the collection process and was being removed during the test. To evaluate this possibility, the sample was taken out of the vacuum chamber after several tests of the sample to allow adsorbed gases to collect on the insulator surface. When the sample was tested after an overnight exposure to the atmosphere, results similar to those obtained with samples not exposed to atmosphere were found. The effect therefore did not appear to be due to adsorbed gases.

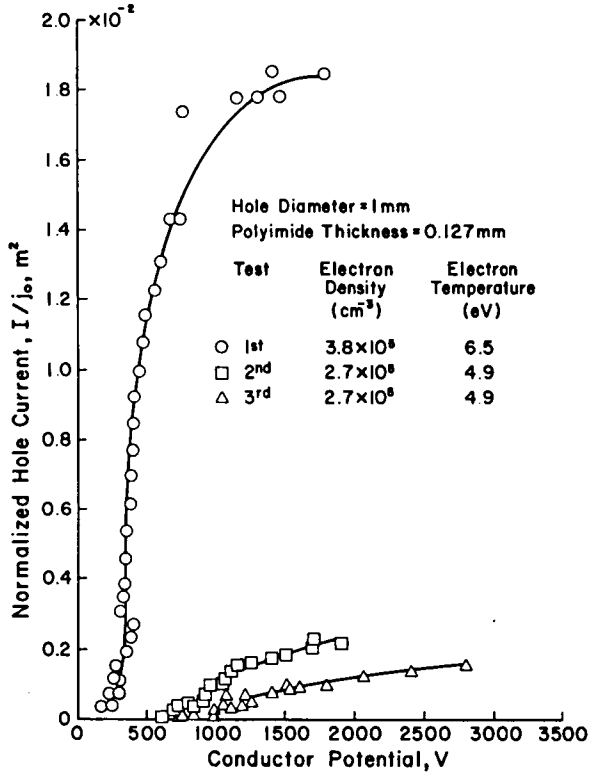


Fig. 4. Comparison between the first, second and third tests of a sample.

On visual inspection of samples after tests, it was observed that there was some discoloration of the insulating material about the hole, and the interior of the hole itself appeared smoother and more polished than it did immediately after drilling or punching the hole. It was found that previously tested holes could be made to increase their current collection by merely mechanically scraping the interior of the hole. This scraping was accomplished with a drill bit and resulted in no significant change in hole diameter. The effect of scraping can be seen in Fig. 5. A possible explanation of this effect is that the interior of the hole and the area immediately surrounding the hole is altered by the energetic bombardment of electrons, and that scraping the interior of the hole restores the hole to its approximate former state. The increased current collection points out that the condition of the hole is an important part of the collection mechanism.

Surface Roughening. Because the condition of the surface appears to be important to the collection process, the flat insulator surfaces were scribed with a sharp metal stylus. This was done to give a better understanding of the effect of surface condition. Three scribed patterns were used: orthogonal lines (two sets of parallel lines at right angles to each other); radial lines originating from the vicinity of the hole; and concentric circles with the hole

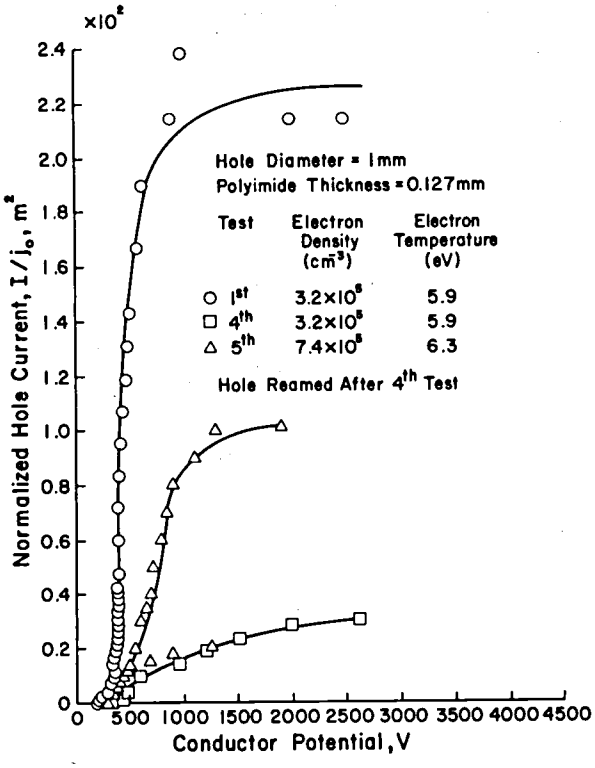


Fig. 5. Comparison of current characteristics of a single hole in three conditions, fresh, old, and reamed.

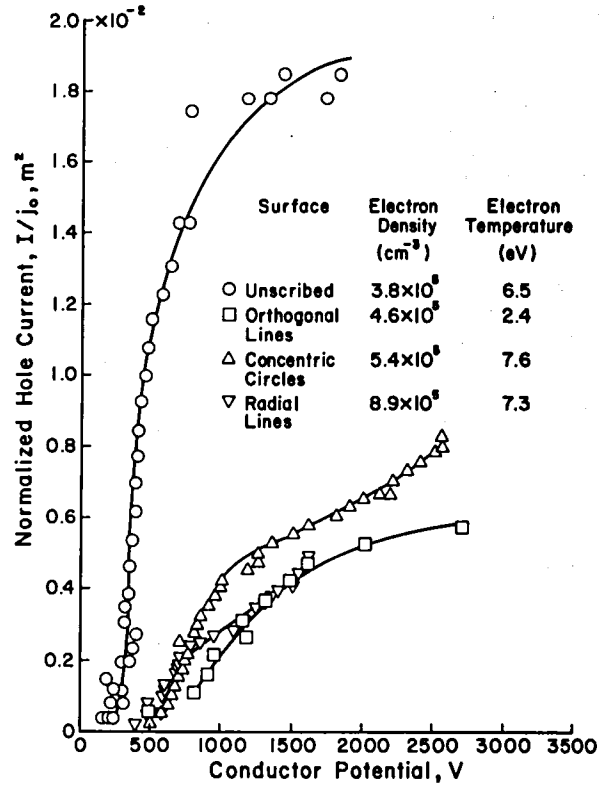


Fig. 6. Comparison of a flat surface sample with samples having scribed patterns.

at the common center. As seen from Fig. 6, there is a significant reduction in the current collected by the scribed surfaces. A possible explanation of this effect appears to be that secondary electron emission is reduced by roughening a surface.[9] Secondary electron emission has been proposed as a collection mechanism by previous investigations.[1,5]

Variation of Temperature. To test for the effect of temperature, the samples were heated to five different temperatures: 27°, 47°, 70°, 95°, and 120°C. There was a general reduction in collected current with increasing temperature, see Fig. 7. By crossplotting the faired curves of Fig. 7, a temperature variation was found as a function of conductor potential, this is shown in Fig. 8. This effect seems to indicate a multi-step secondary electron emission process. For insulators, secondary electron emission has a temperature variation of $T^{-1/2}$ under electron bombardment.[10] With the probability of a single secondary electron emission event proportional to $T^{-1/2}$, the larger negative powers in Fig. 7 can be thought of as resulting from a number of secondary electron events in series. The increased negative powers at higher collection voltages further implies a larger number of secondary electron events in this series.

Variation of Current Collection with Time. All previous tests reported herein were for short durations, lasting at most a few minutes. A more extended test was conducted to determine the evolution that takes place with more prolonged electron collection. Figure 9 shows that

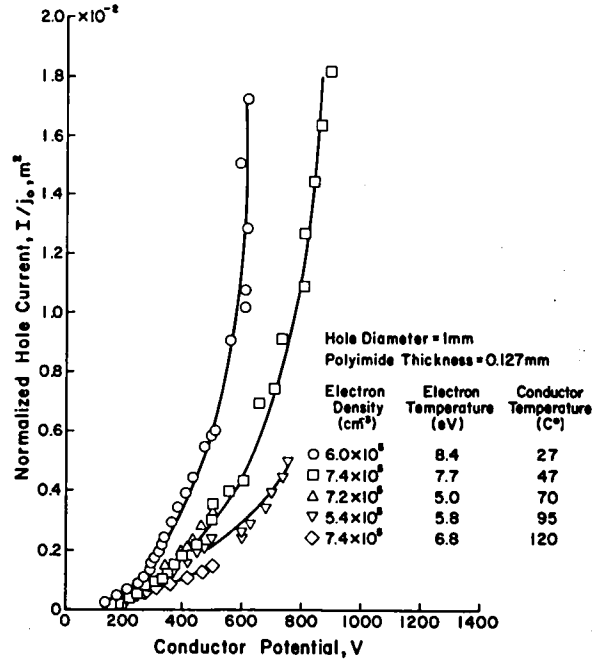


Fig. 7. The effect of sample temperature on electron collection.

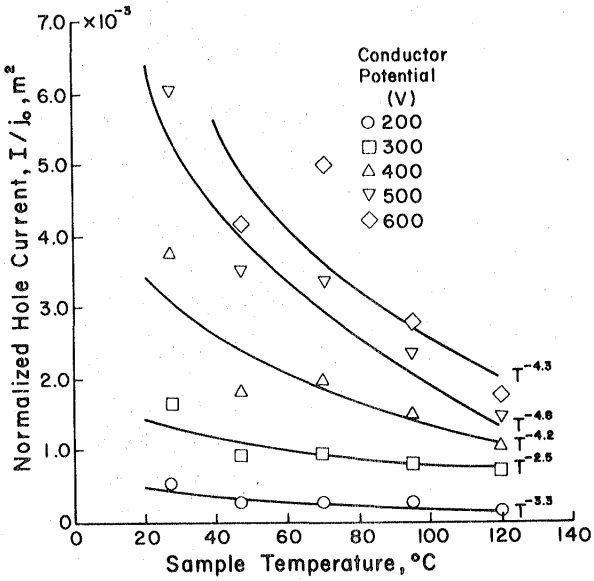


Fig. 8. Data of Fig. 7 plotted to show the effect of conductor temperature at constant conductor potentials.

the collected current does not decrease continuously with time, but shows occasional transients of large magnitude, often followed by gradual decreases. A visual inspection of the sample after the test showed that the polyimide insulator was darkened and beveled near the hole, as indicated in Fig. 10. The blackening and beveling of the sample supports the conclusion that, in time, the insulator is degraded by the energetic bombardment of electrons. This degradation should be included in any estimate of long-term collection effects in space.

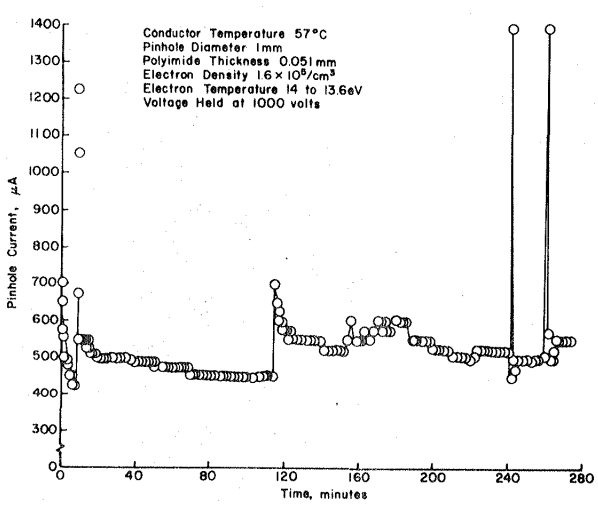


Fig. 9. Long-term variation of electron current collection with time at constant potential.

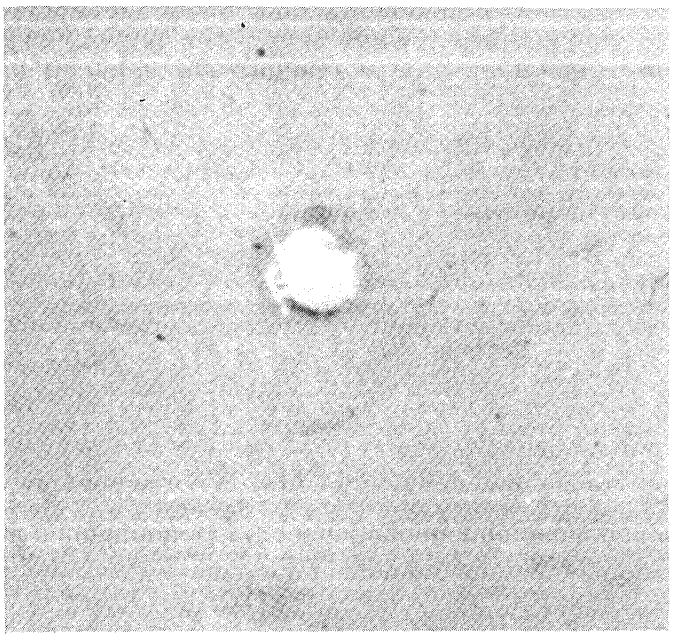

(a)

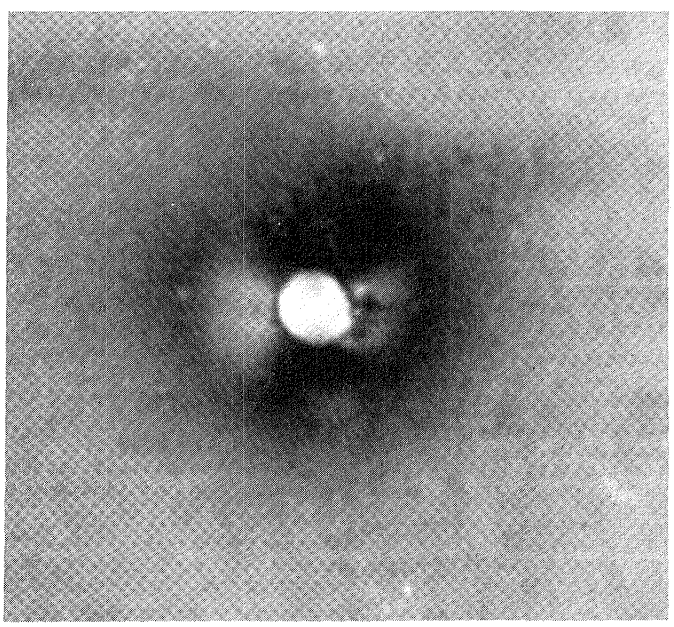

(b)

Fig. 10. Effect of current collection on insulator appearance, (a) untested (b) after 375 min.

Variation of Insulator Thickness. Two insulator thicknesses were tested, 0.051 mm and 0.127 mm. These were tested using four hole sizes: 0.35, 0.52, 1.0 and 2.0 mm diameter. For the samples tested there was no significant difference in current collection. It should be noted, though, that the insulator thickness was small relative to the hole diameter for all configurations tested.

Effect of Insulator Area. An insulator area effect had been found in an earlier investigation.[5] Tests were conducted to look for a similar effect in this investigation. To test for an area effect, three samples were constructed: 2 × 2 cm, 5 × 5 cm, and 12 × 12 cm samples. These samples gave a surface area range of 4 $cm^2$ to 144 $cm^2$. The results of these tests are shown in Fig. 11. From this figure, it is seen that there is some area effect. The effect shown in Fig. 11, though, is smaller than that reported earlier by Kennerud.[5] The normalized results shown lie within the extremes of his data which exhibit a much sharper rise in current collection with insulator area surrounding the hole. This difference is possibly due to the experimental differences mentioned earlier.

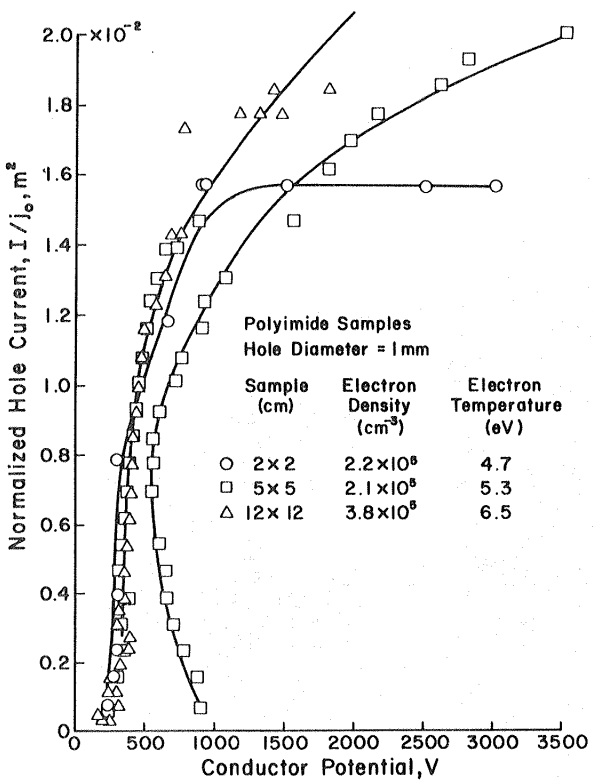


Fig. 11. Comparison of samples with different insulator surface areas.

Negative Bias

Normalization. Since ion collection involves different charge carriers than electron collection, a different normalization procedure should be expected. The current density of ions arriving at a planar boundary is given by the Bohm current density,[11]

$$j_{Bohm} = ne\left[\frac{kT_e}{m_i}\right]^{1/2} \qquad (2)$$

where $m_i$ is the ion mass and all other parameters are as defined previously. The gas used for the hollow cathode (argon) is assumed for $m_i$. As will be shown, a simple exchange of this current density for random electron current density did not result in adequate correlation of ion collection data.

Effect of Pinhole Size. Four hole diameters were tested: 2.0, 2.95, 4.1 and 4.99 mm. The selection of such large hole sizes were based largely on the small ion currents collected. The data of these tests were normalized using both the Bohm current density, $j_{Bohm}$, and the Bohm current, $I_{Bohm} = A_{hole} j_{Bohm}$, see Figs. 12(a) and 12(b). These results show that, unlike positive bias, hole area is an important parameter for ion current collection. Also, for the voltage range covered, the ion current collected varied nearly linearly with negative voltage. Preliminary tests at larger negative voltages than 1000 V have shown large, rapid, and variable current increases. The trends indicated in Figs. 12(a) and 12(b) should therefore not be extrapolated beyond the range shown.

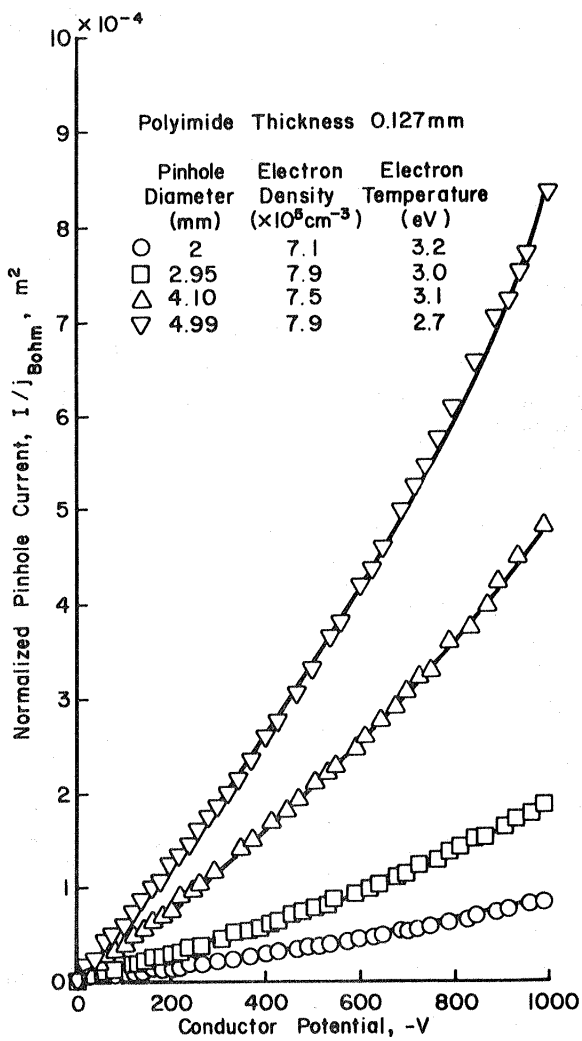


(a)

Fig. 12. Ion current collection characteristics for a range of hole sizes, normalized by (a) $j_{Bohm}$ (b) $I_{Bohm}$.

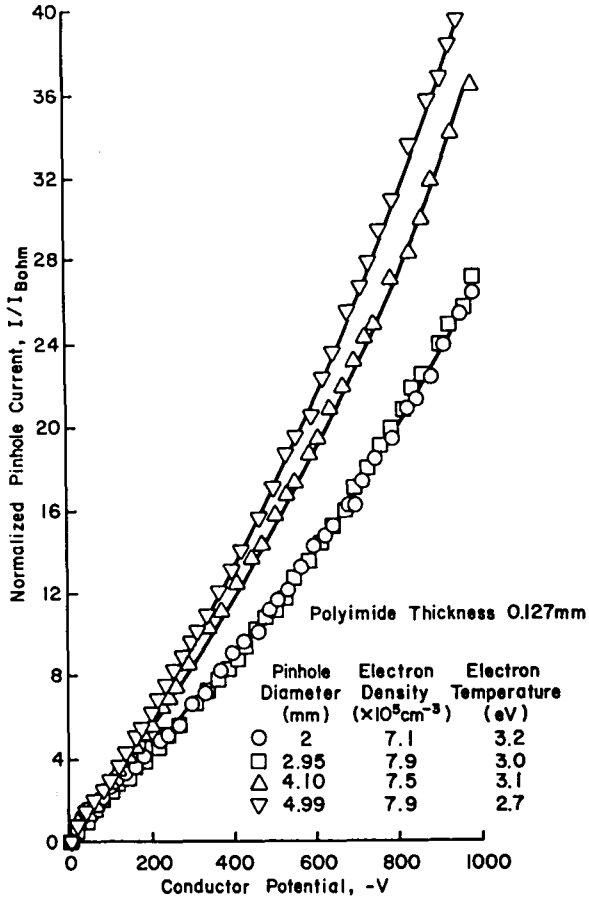


(b)

Fig. 12. Continued.

Modeling

For positive bias (electron collection), a crude model has been developed. This model is for the current collection process before any high-current mode change occurs as discussed earlier. It is assumed that any glow discharge effects are negligible in this lower voltage region, and that the collection process involves only electrostatic collection from the plasma and a collection enhancement due to secondary electron emission on the insulator surface. The model is described by

$$I = j_o \left[1 + \frac{b^2}{4} + (1 - \frac{b^2}{4})\frac{V}{kT_e}\right] \times \left[A_{hole} + A_{eff} \left(\frac{298}{T}\right) \xi(V)\right] \quad (3)$$

The term $j_o\left[1 + \frac{b^2}{4} + (1 - \frac{b^2}{4}) \frac{V}{kT_e}\right]$ is the collection term found by Parker and Whipple for collection by a planar probe surrounded by a conductor.[12] The b in this term is a constant, found to be about 1.8 for the test environment used herein. V is the conductor potential, k is Boltzmann's constant, $T_e$ is the electron temperature, and $j_o$ is the random current density. The term $A_{hole}$ is the area of exposed conductor. The term $A_{eff}$ $(298/T)\xi(V)$ takes into account the collection involving secondary electron emission that gives the temperature dependence of the secondary electron emission, where T is the sample temperature (in °K), and

$$\xi(V) = 2.1 + 4.3 \times 10^{-3}\ V\ , \quad (4)$$

found experimentally. The term $A_{eff}$ is the area of insulation around the hole that contributes to the electron current collection, it also includes the effect of the secondary electron emission coefficient at 298°K. $A_{eff}$ is assumed as a function of only conductor potential. Using this model, the effective radius, $r_{eff}$, as measured from the hole edge, was calculated from the data and is shown in Fig. 13. The calculated values of radius were then fitted to a simple parabolic variation with potential. The best least-square fit was obtained with

$$r_{eff} = 3.46 \times 10^{-8}\ V^2\ . \quad (5)$$

This empirical fit was then used to calculate expected current/voltage curves. Typical calculated curves are shown in Fig. 14(a) and 14(b), together with the corresponding experimental data.

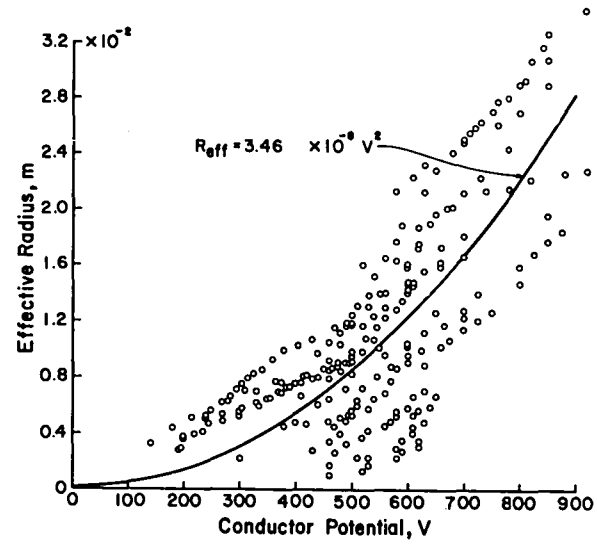


Fig. 13. Effective collection radius as a function of conductor potential.

For negative bias (ion collection), the data in the voltage region investigated is in approximate agreement with the expression found by Parker and Whipple for a planar probe,[12]

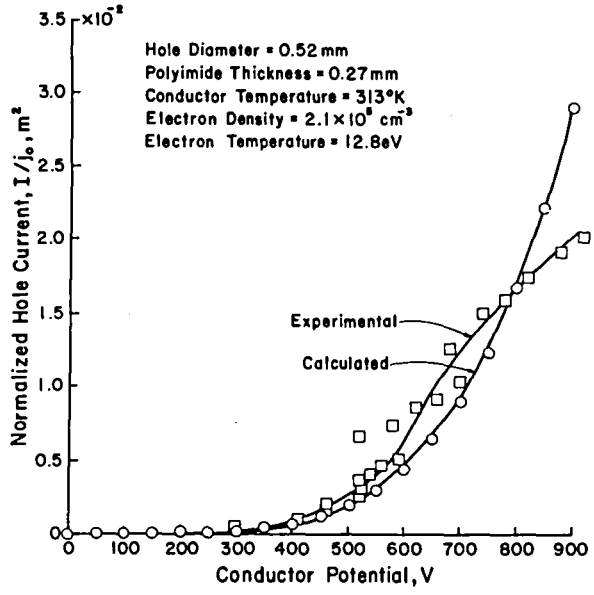


(a)

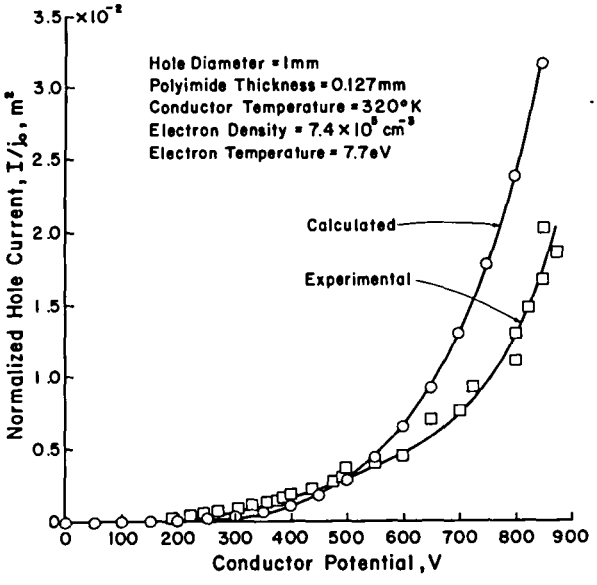


(b)

Fig. 14. Comparison of experimental and calculated electron current collection characteristics.

$$I = I_{Bohm}\left[1 + \frac{V}{E_o} - \frac{b^2}{4}\frac{V^2}{E_o(E_o+V)}\right] \qquad (6)$$

where $E_o = 8\ kT_e$. This agreement is shown in Fig. 15 for different values of b. Note that the collection area for ions is simply the area of the hole. For the low voltage data presented for ion collection, this simple modeling technique appears adequate.

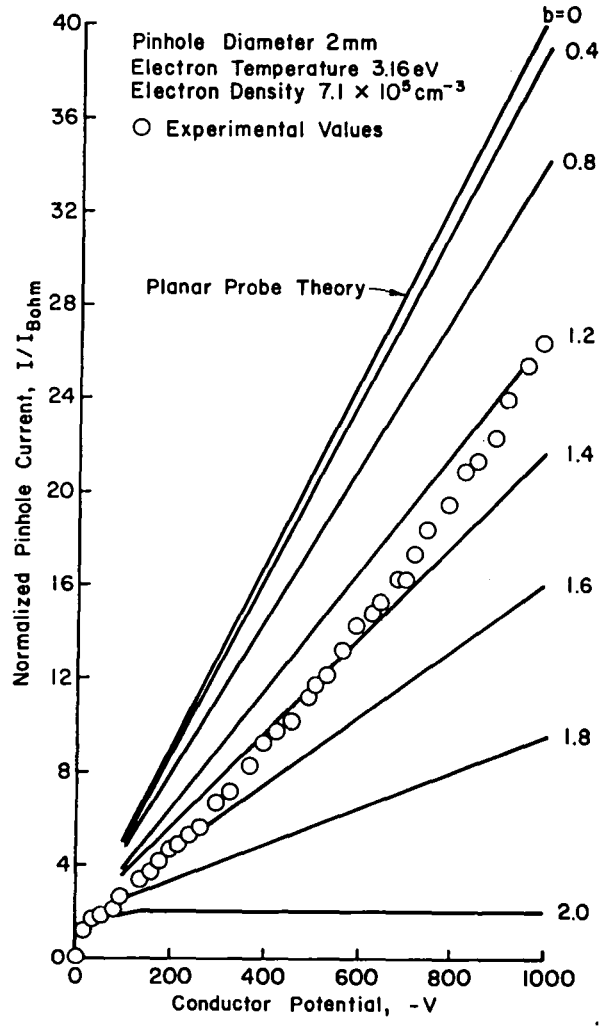


Fig. 15. Comparison of experimental ion current collection characteristics with planar probe theory (parameter b is an adjustable parameter of the probe theory).

## Concluding Remarks

In this investigation, two processes have been found to add to the current collection mechanism for positive bias. These were secondary electron emission by the insulator surface surrounding the surface defect made apparent by the temperature dependence, and at higher voltages a glow discharge effect. The evidence supporting the secondary electron emission are the temperature effect and the effect of roughening the insulator surface. The glow discharge effect was easily seen at high currents, and the change of mode is probably related to some breakdown in the neutral background gas. Previous investigations where lower background pressures were used ($<10^{-6}$ Torr), did not report this effect.[1,5]

A model using secondary electron emission for the enhancement of current collection area has been developed. The empirical fit used for area enhancement gives a reasonable agreement to experimental results. Because of the empirical fit used, a change in insulator materials would require additional data for model verification.

Negative bias experiments were done in a low voltage region where experimental results were consistent and agreed with planar probe theory. Although data were not presented at higher negative voltages, currents at these higher voltages were highly variable, with rapid transients that tended to damage instrumentation.

## Acknowledgement

Work described in this paper was supported by NASA grant NSG 3196.

## References

1. Cole, R. K., Ogawa, H. S., and Sellen, J. M., Jr., "Operation of Solar Cell Arrays in Dilute Streaming Plasmas," AIAA 7th Electric Propulsion Conference, Williamsburg, Virginia, Paper No. 69-262 (March 1969).
2. Grier, N. T. and McKinzie, D. J., "Current Drainage to a High Voltage Probe in a Dilute Plasma," AIAA 10th Aerospace Sciences Meeting, San Diego, California, Paper No. 72-105 (January 1972).
3. Bayless, J. R., Herron, B. G., and Worden, J. D., "High Voltage Solar Array Technology," AIAA 9th Electric Propulsion Conference, Bethesda, Maryland, Paper No. 72-443 (April 1972).
4. Domitz, S. and Grier, N. T., "The Interaction of Spacecraft High Voltage Power Systems with the Space Plasma Environment," NASA Technical Memorandum TMX-71554 (June 1974).
5. Kennerud, K. L., "High Voltage Solar Array Experiments," NASA Contract Report CR-121280 (March 1974).
6. Kaufman, H. R. and Isaacson, G. C., "The Interactions of Solar Arrays with Electric Thrusters," AIAA International Electric Propulsion Conference, Key Biscayne, Florida, Paper No. 76-1051 (November 1976).
7. Burrowbridge, D. R., "A Technique for Simulating the Ionospheric Plasma," NASA-Goddard Space Flight Center Report No. TMX-36226 (May 1968).
8. Chen, F. F., Introduction to Plasma Physics, Plenum Press, New York, p. 202, 1977.
9. Rashkovski, S. F., "Secondary Emission from Rough Surfaces," Radio Engng. Electron Physics 3, pp. 97-117 (1958).
10. Gibbons, D. J., "Secondary Electron Emission," in Handbook of Vacuum Physics, Vol. 2, Physical Electronics (A. H. Beck, ed.), Pergammon Press, Glasgow, Scotland, pp. 301-395 (1966).
11. Chen, F. F., Introduction to Plasma Physics, Plenum Press, New York, p. 246, 1977.
12. Parker, L. W. and Whipple. E. C., "Theory of a Satellite Electrostatic Probe," Annals of Physics 44, pp. 126-167 (1967).

## APPENDIX B. SECONDARY ELECTRON EMISSION FROM INSULATORS

It has been believed that secondary electron emission from the insulating material surrounding the hole contributes to the electron collection mechanism[1,2] (see Appendix A). With this in mind, modeling of the electron collection process will necessarily include some of the secondary emission properties. This appendix is a brief review of the properties that have been, or are felt to be, important to future modeling needs.

Secondary Electron Emission Yields. Secondary emission yields consist of two components, true secondary electrons (emerging electrons with energy less than 50 eV) and backscattered primaries.[3] The secondary emission yield is given by the ratio

$$\sigma = \frac{\text{number of emitted electrons}}{\text{number of incident electrons}} \quad . \tag{B-1}$$

This total yield can also be written as

$$\sigma = \delta + \eta \quad , \tag{B-2}$$

where $\delta$ is the yield of true secondaries

$$\delta = \frac{\text{number of true secondary electrons emitted}}{\text{number of incident electrons}} \tag{B-3}$$

and $\eta$ is the backscattered yield

$$\eta = \frac{\text{number of backscattered electrons}}{\text{number of incident electrons}} \quad . \tag{B-4}$$

The total yield is dependent on the incident electron energy, but $\delta$ and $\eta$ exhibit different dependencies.

In the present investigation, the insulating materials of interest are polyimide and polytetrafluoroethylene (teflon). Studies of emission yields ($\sigma$) of these materials have been done by Willis and Skinner.[4] The secondary emission yield ($\delta$) of polyimide has been investigated by Leung, Tueling and Schnauss.[5] The emission yield ($\sigma$) for polyimide from Willis and Skinner (angle of incidence of primary electrons not given) and the secondary yield ($\sigma$) from Leung, Tueling and Schnauss (for normal incidence) are shown in Fig. B-1.

The emission yields from Willis and Skinner have been fit to the form[6]

$$\sigma(E) = K \left(e^{-aE} - e^{-bE}\right) \tag{B-5}$$

where E is the energy of the primary electron in eV and K, a and b are constants dependent on the material. For polyimide, K = 3.5, $a = 2 \times 10^{-3}$ and $b = 1.5 \times 10^{-2}$, and for polytetrafluorethylene (teflon) K = 5.8, $a = 1 \times 10^{-3}$ and $b = 5 \times 10^{-3}$. The secondary yield from Leung, Tueling and Schnauss is given by

$$\delta(E) = \frac{E}{E_{II}} \exp \frac{-2}{E_{max}^{1/2}} \left(E^{1/2} - E_{II}^{1/2}\right) \tag{B-6}$$

where $E_{max}$ is the primary energy where $\delta$ is maximum (250 eV for polyimide) and $E_{II}$ is the primary energy where $\delta = 1$ (the second crossover point, $E_{II}$ = 1000 eV for polyimide, see Fig. B-1). All energies are in eV. Please note that since the primary electron reflection coefficient $\eta$ can vary between 0 and 1, $\sigma$ should at all times be greater than $\delta$. The amount by which this is not true for the data described (Fig. B-1) indicates the probable error in this data.

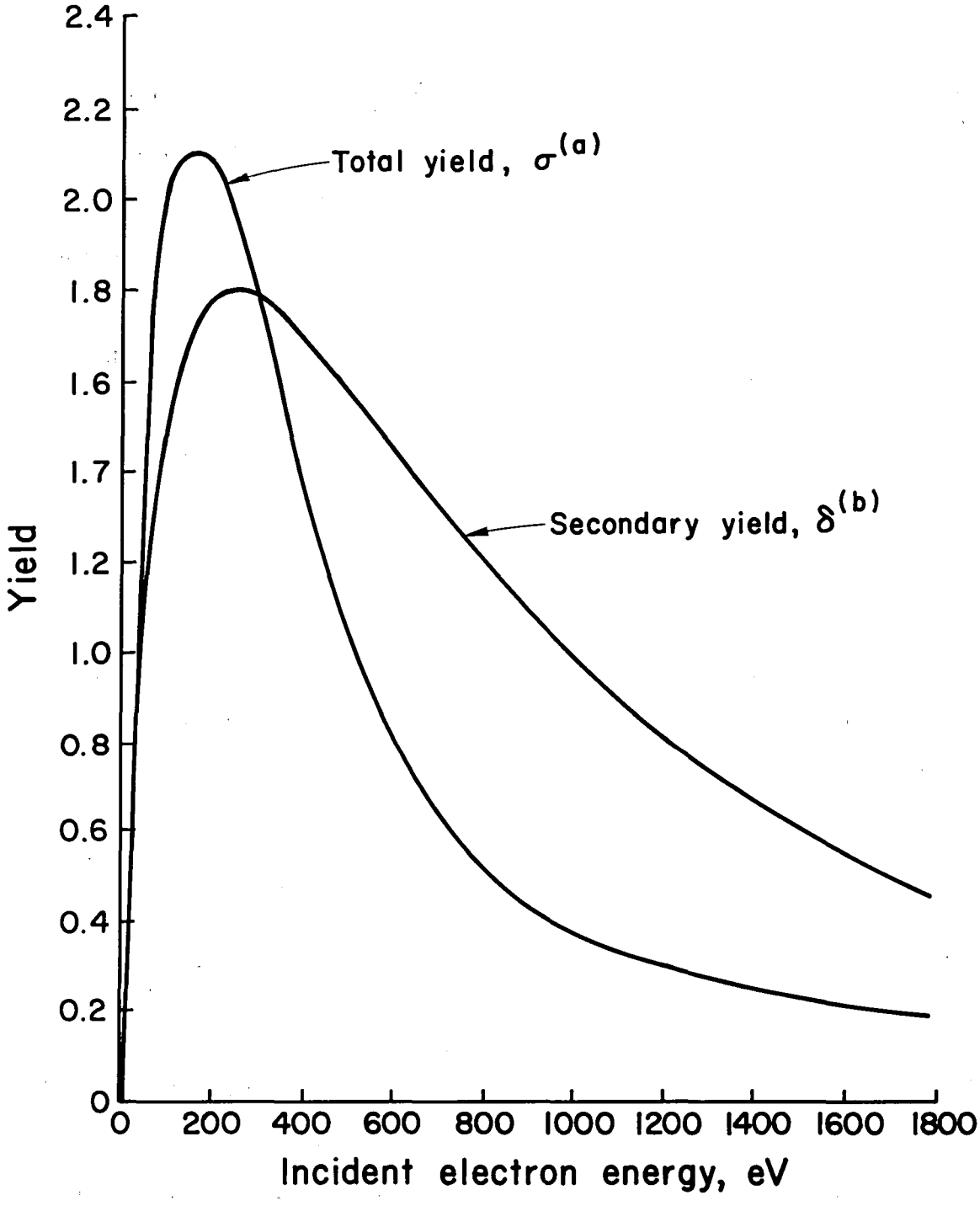


Fig. B-1. (a) Total yield from Willis and Skinner[4] and (b) secondary electron yield from Leung, Tueling and Schnauss[5] as a function of incident electron energy.

Angular Dependence of Secondary Emission Yields. Secondary emission yields are dependent on the incidence angle of the primary electrons. This dependence is given by[9]

$$\delta_\theta = \delta_o e^{p(1 - \cos\theta)} \tag{B-9}$$

where $\theta$ is the angle of incidence of electrons with respect to the surface normal, $\delta_o$ is the secondary emission yield at normal incidence, $\delta_\theta$ is the secondary emission yield for electrons incident at an angle $\theta$, and p is a constant of the material independent of $\theta$. The constant p is related to the mean depth of penetration of primary electrons and the absorption coefficient of secondary electrons. It has been determined empirically to be approximately 2 for most polymers.[8]

Energy Distribution of Secondary Electrons. A typical energy distribution is shown in Fig. B-2. Although this distribution is for a metal, many insulators have been found to have similar distributions.[10] The energy distributions have been found to be independent of primary electron energy range of 20 to 1000 eV.[11]

Angular Distribution of Secondary Electrons. The secondary electrons are emitted from the surface with approximately a cosine distribution[12] which is nearly independent of the angle of incidence of the primary electrons.

Effect of Temperature. The secondary yield has been found to have a temperature dependence for insulators,[13] although not for metals.[11] The reason for this difference appears to be in the energy loss mechanism of the secondary electrons in the material. In metals, the secondaries

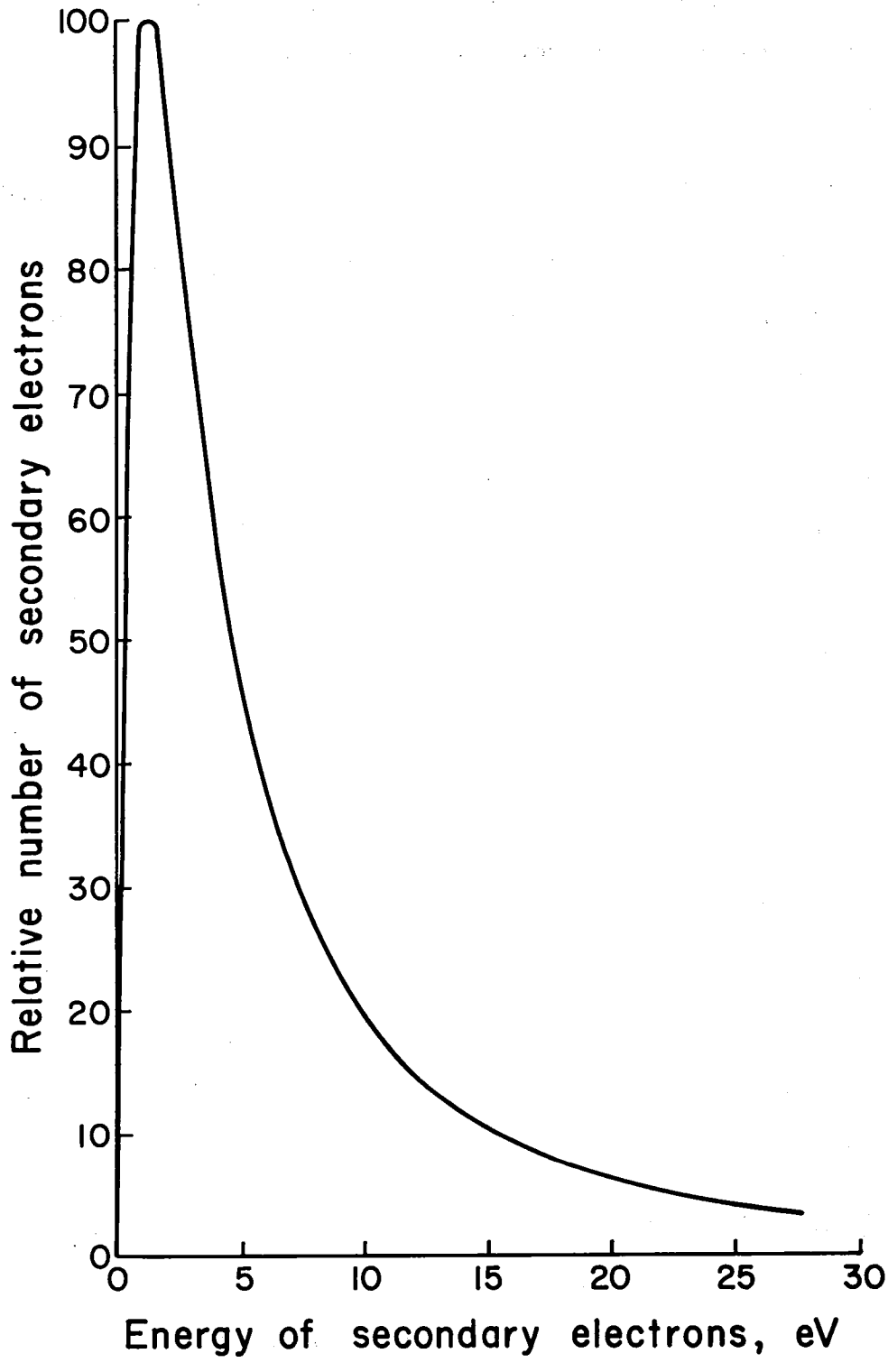


Fig. B-2. Energy distribution of secondary electrons for tantalum.[9]

can collide with free and bound electrons involving large and small amounts of energy transfer. In insulators, because of the large gap between the valence and conduction bands, any energy loss mechanism of the secondaries must depend on electron collisions with lattice defects and/or electron-phonon interactions for energies less than the band gap.[11] For ionic crystals, a temperature dependence of

$$\frac{\delta_1}{\delta_2} = \left\{ \frac{\dfrac{2}{e^{h\nu/kT_2} - 1} + 1}{\dfrac{2}{e^{h\nu/kT_1} - 1} + 1} \right\}^{1/2} \tag{B-8}$$

has been derived,[14] and is in good agreement with experimental results. In the expression, h is Planck's constant, k is Boltzmann's constant, T is the insulator temperature and $\nu$ is the frequency of optical vibrations. For $kT \gg h\nu$, this expression (Eq. B-8) becomes

$$\frac{\delta_1}{\delta_2} \approx \sqrt{\frac{T_2}{T_1}} \tag{B-9}$$

which has been mentioned in a previous report.[2]

Non-polar insulators have a temperature dependence of[15]

$$\frac{\delta_1}{\delta_2} = \left[ \frac{\displaystyle\int_o^{\nu_{max}} \left( \frac{2}{e^{h\nu/kT_2 - 1}} + 1 \right) \nu^2 d\nu}{\displaystyle\int_o^{\nu_{max}} \left( \frac{2}{e^{h\nu/kT - 1}} + 1 \right) \nu^2 d\nu} \right]^{1/2} \tag{B-10}$$

For $kT \gg h\nu$, this expression reduces to Eq. B-9.

Effect of Surface Condition. It has been found that when a surface is roughened, the secondary yield decreases.[16] The explanation for this is that when a surface is roughened, microscopic Faraday spaces (spaces without fields and from which no secondary electrons can be emitted) are formed. Thus decreasing the total area from which emission may occur.[16] This effect has also been mentioned in a previous report.[2]

# REFERENCES

## SECTION I


1. D. J. Santeler, D. H. Hokeboer, D. W. Jones, and F. Pagaro, "Vacuum Technology and Space Simulation," NASA Special Publication SP-105, pp. 33-40, 1967.

2. J. H. Wolfe, in "Solar Wind" (edited by C. P. Sonett, P. J. Coleman, Jr., and J. M. Wilcox), NASA Special Publication SP-308, pp. 170-201, 1972.

3. C. R. Chappell, Rev. of Geophysics and Space Physics, Vol. 10, pp. 951-979, Nov. 1972.

4. R. K. Cole, H. S. Ogawa and J. M. Sellen, Jr., "Operation of Solar Cell Arrays in Dilute Streaming Plasmas," AIAA Paper No. 69-262, March 1969.

5. N. T. Grier and D. J. McKinzie, "Current Drainage to a High Voltage Probe in a Dilute Plasma," AIAA Paper No. 72-105, January 1972.

6. J. R. Bayless, B. G. Herron and J. D. Worden, "High Voltage Solar Array Technology," AIAA Paper No. 72-443, April 1972.

7. S. Domitz and N. T. Grier, "The Interaction of Spacecraft High Voltage Power Systems with the Space Plasma Environment," NASA Technical Memorandum TMX-71554, June 1974.

8. K. L. Kennerud, "High Voltage Solar Array Experiments," NASA Contr. Rep. CR-121280, March 1974.

9. H. R. Kaufman and R. S. Robinson, "Interaction of High Voltage Surfaces with the Space Plasma," NASA Contr. Rep. CR-165131, May 1980.

10. H. R. Kaufman and R. S. Robinson, "Interaction of High Voltage Surfaces with the Space Plasma," NASA Contr. Rep. CR-159731, May 1979.

11. R. P. Stillwell, H. R. Kaufman and R. S. Robinson, "Experimental Simulation of Space Plasma Interactions with High Voltage Solar Arrays," AIAA Paper No. 81-0741, April 1981.

12. T. P. Armstrong, R. C. Chaky, J. Enock, J. H. Nonrast and G. G. Wiseman, "Self-Consistent Numerical Simulation of Plasma-Insulator Interactions," NASA Research Grant NSG-3290, Univ. of Kansas, August 1980.

## SECTION II


1. H. R. Kaufman and R. S. Robinson, "Interaction of High Voltage Surfaces with the Space Plasma," NASA Contr. Rep. CR-165131, May 1980.

2. H. R. Kaufman and G. C. Isaacson, "The Interactions of Solar Arrays with Electric Thrusters," AIAA Paper No. 76-1051, November 1976.

3. D. R. Burrowbridge, "A Technique for Simulating the Ionospheric Plasma," NASA Goddard Space Flight Center Report No. TMX-36226, May 1968.

4. H. R. Kaufman and R. S. Robinson, "Interaction of High Voltage Surfaces with the Space Plasma," NASA Contr. Rep. CR-159731, May 1979.


## SECTION III


1. Martin A. Uman, Introduction to Plasma Physics, New York, McGraw Hill, Inc., pp. 19-22, 1964.

2. H. R. Kaufman and R. S. Robinson, "Interaction of High Voltage Surfaces with the Space Plasma," NASA Contr. Rep. CR-165131, May 1980.

3. H. R. Kaufman and R. S. Robinson, "Interaction of High Voltage Surfaces with the Space Plasma," NASA Contr. Rep. CR-159731, May 1979.

4. K. L. Kennerud, "High Voltage Solar Array Experiments," NASA Contr. Rep. CR-121280, March 1974.


## SECTION IV


1. L. W. Parker and E. C. Whipple, "Theory of a Satellite Electrostatic Probe," Annals of Physics 44, pp. 126-167 (1967).

2. H. R. Kaufman and R. S. Robinson, "Interaction of High Voltage Surfaces with the Space Plasma," NASA Contr. Rep. CR-159731, May 1979.

3. M. A. Uman, Introduction to Plasma Physics, New York, McGraw Hill, Inc., pp. 19-22, 1964.

4. H. R. Kaufman and R. S. Robinson, "Interaction of High Voltage Surfaces with the Space Plasma," NASA Contr. Rep. CR-165131, May 1980.

5. J. D. Jackson, Classical Electrodynamics, 2nd Ed., New York, John Wiley and Sons, Inc., pp. 27-53, 1975.

6. F. F. Chen, Introduction to Plasma Physics, New York, Plenum Press, pp. 248-249, 1977.

## SECTION V

1. K. L. Kennerud, "High Voltage Solar Array Experiments," NASA Contr. Rep. CR-121280, March 1974.

## APPENDIX A

1. R. P. Stillwell, H. R. Kaufman and R. S. Robinson, "Experimental Simulation of Space Plasma Interactions with High Voltage Solar Arrays," AIAA Paper No. 81-0741, April 1981.

## APPENDIX B

1. R. K. Cole, H. S. Ogawa and J. M. Sellen, Jr., "Operation of Solar Cell Arrays in Dilute Streaming Plasma," AIAA Paper No. 69-262, March 1969.

2. H. R. Kaufman and R. S. Robinson, "Interaction of High Voltage Surfaces with the Space Plasma," NASA Contr. Rep. CR-165131, May 1980.

3. E. A. Burke, "Secondary Emission from Polymers," IEEE Transactions on Nuclear Science 6, pp. 1760-1764 (1980).

4. R. F. Willis and D. K. Skinner, "Secondary Electron Emission Yield Behavior of Polymers," Solid State Communications 13, pp. 685-688 (1973).

5. M. S. Leung, M. B. Tueling and E. R. Schnauss, "Effects of Secondary Electron Emission on Charging," Spacecraft Charging Technology Conference, Colorado Springs, Colorado, Nov. 12-14, 1980.

6. J. W. Haffner, "Secondary Electron Effects on Spacecraft Charging," Spacecraft Charging Technology, NASA Conference Publication 2071, AFG L-TR-79-0082, pp. 756-768 (1978).

7. H. Bruining, "Secondary Electron Emission, Part II. Absorption of Secondary Electrons," Physica 5, pp. 901-912 (1938).

8. J. A. Wall, E. A. Burke and A. R. Frederickson, "Results of Literature Search on Dielectric Properties and Electron Interaction Phenomena Related to Spacecraft Charging," Proceeding of the Spacecraft Charging Technology Conference, NASA TMX-73537, AFGL-TR-77-0051, pp. 569-591 (1977).

9. R. Kollath, "On the Energy Distribution of Secondary Electrons," Ann. Phys. Lpz. 39, pp. 59-80 (1941).

10. H. Bruining, Physics and Applications of Secondary Electron Emission, New York, McGraw Hill, Inc., pp. 97-108, 1954.

11. D. J. Gibbons, "Secondary Electron Emission," Handbook of Vacuum Physics, Vol. 2, Physical Electronics (A. H. Beck, ed.), Pergammon Press, Glasgow, Scotland, pp. 301-395 (1966).

12. J.L.H. Jonker, "The Angular Distribution of the Secondary Electrons of Nickel," Philips Res. Rep. 6, pp. 372-387 (1951).

13. J. B. Johnson and K. G. McKay, "Secondary Electron Emission of Crystalline MgO," Phys. Rev. 91, pp. 582-587 (1953).

14. A. J. Dekker, "Energy and Temperature Dependence of the Secondary Emission of MgO," Phys. Rev. 94, pp. 1179-1182 (1954).

15. A. J. Dekker, "On the Escape Mechanism of Secondary Electrons from Insulators," Physica 21, pp. 29-38 (1954).

16. S. F. Rashkovskii, "Secondary Emission from Rough Surfaces," Radio Engng. Electron Physics 3, pp. 97-118 (1958).

# DISTRIBUTION

| | Copies |
|---|---|
| National Aeronautics and Space Administration<br>Washington, DC 20546 | |
| Attn: RS/Mr. Dell Williams, III | 1 |
| RTS-6/Mr. Wayne Hudson | 1 |
| RTS-6/Mr. Jerome Mullin | 1 |
| MT/Mr. Ivan Bekey | 1 |
| National Aeronautics and Space Administration<br>Lewis Research Center<br>21000 Brookpark Road<br>Cleveland, OH 44135 | |
| Attn: Research Support Procurement Section | |
| Mr. G. Golinski, MS 500-306 | 1 |
| Technology Utilization Office, MS 3-19 | 1 |
| Report Control Office, MS 5-5 | 1 |
| Library, MS 60-3 | 2 |
| Mr. N. Musial, MS 500-113 | 1 |
| Dr. M. Goldstein, Chief Scientist, MS 5-3 | 1 |
| Mr. T. Cochran, MS 501-8 | 1 |
| Mr. D. Petrash, MS 501-5 | 1 |
| Mr. N. Grier, MS 501-7 | 30 |
| Mr. M. Mirtich, MS 501-7 | 1 |
| Mr. R. Finke, MS 77-4 | 1 |
| Mr. B. Banks, MS 501-7 | 1 |
| Mr. D. Byers, MS 501-7 | 1 |
| Mr. W. Kerslake, MS 501-7 | 1 |
| Mr. V. Rawlin, MS 501-7 | 1 |
| National Aeronautics and Space Administration<br>Marshall Space Flight Center<br>Huntsville, AL 35812 | |
| Attn: Mr. Jerry P. Hethcoate | 1 |
| Mr. John Harlow | 1 |
| Mr. John Brophy | 1 |
| Mr. Robert T. Bechtel | 1 |
| Mr. M. Ralph Carruth, Jr. | 1 |
| NASA Scientific and Technical<br>Information Facility<br>P.O. Box 8757<br>Baltimore, MD 21240 | |
| Attn: Accessioning Department | 1 |

National Aeronautics and Space Administration
Goddard Space Flight Center
Greenbelt, MD 20771
Attn: Mr. W. Isley, Code 734 1
Mr. A. A. Vetman 1
Dr. David H. Suddeth 1

National Aeronautics and Space Administration
Ames Research Center
Moffett Field, CA 94035
Attn: Technical Library 1

National Aeronautics and Space Administration
Langley Research Center
Langley Field Station
Hampton, VA 23365
Attn: Technical Library 1
Mr. B. Z. Henry 1

The Aerospace Corporation
P.O. Box 95085
Los Angeles, CA 90045
Attn: Dr. B. A. Haatunion 1
Mr. A. H. Silva 1

The Aerospace Corporation
Space Sciences Laboratory
P.O. Box 92957
Los Angeles, CA 90009
Attn: Dr. Y. T. Chiu 1

Bell Laboratories
600 Mountain Avenue
Murray Hill, NJ 07974
Attn: Dr. Edward G. Spencer 1
Dr. Paul H. Schmidt 1

Boeing Aerospace Company
P.O. Box 3999
Seattle, WA 98124
Attn: Mr. Donald Grim, MS 8K31 1
Mr. Russell Dod 1

Case Western Reserve University
10900 Euclid Avenue
Cleveland, OH 44106
Attn: Dr. Eli Reshotko 1

C.E.N.-F.A.R.
Service Du Confinement Des Plasmas
BP6
92260 Fontenay-Aux-Roses,
FRANCE
Attn: J. F. Bonnal 1

Circuits Processing Apparatus, Inc.
725 Kifer Road
Sunnyvale, CA 94086
Attn: Spencer R. Wilder 1

Commonwealth Scientific Corporation
500 Pendleton Street
Alexandria, VA 22314
Attn: George R. Thompson 1

Computing Center of the USSR Academy of Sciences
Vavilova 40
117333 Moscow, B-333
USSR
Attn: Dr. V. V. Zhurin 1

Comsat Corporation
950 L'Enfant Plaza, S.W.
Washington, DC 20024
Attn: Mr. Sidney O. Metzger 1

COMSAT Laboratories
P.O. Box 115
Clarksburg, MD 20734
Attn: Mr. B. Free 1
Mr. O. Revesz 1

CVC Products
525 Lee Road
P.O. Box 1886
Rochester, NY 14603
Attn: Mr. Georg F. Garfield, Jr. 1

DFVLR - Institut fur Plasmadynamik
Technische Universitat Stuttgart
7 Stuttgart-Vaihingen
Allmandstr 124
WEST GERMANY
Attn: Dr. G. Krulle 1

DFVLR - Institut fur Plasmadynamik
33 Braunschweig
Bienroder Weg 53
WEST GERMANY
Attn: Mr. H. Bessling 1

EG & G Idaho
P.O. Box 1625
Idaho Falls, ID 83401
Attn: Dr. G. R. Longhurst, TSA-104 1

Electro-Optical Systems, Inc.
300 North Halstead
Pasadena, CA 91107
Attn: Dr. R. Worlock 1
Mr. E. James 1
Mr. W. Ramsey 1

Electrotechnical Laboratory
1-1-4, Umezono, Sakura-Mura,
Niihari-Gun
Ibaraki,
JAPAN
Attn: Dr. Katsuya Nakayama 1

Fairchild Republic Company
Farmingdale, NY 11735
Attn: Dr. Domenic J. Palumbo 1

Ford Aerospace Corporation
3939 Fabian Way
Palo Alto, CA 94303
Attn: Mr. Robert C. Kelsa 1

General Dynamics
Kearney Mesa Plant
P.O. Box 1128
San Diego, CA 92112
Attn: Dr. Ketchum 1

Giessen University
1st Institute of Physics
Giessen,
WEST GERMANY
Attn: Professor H. W. Loeb 1

Hughes Aircraft Company
Space and Communication Group
P.O. Box 92919
Los Angeles, CA 90009
Attn: Dr. M. E. Ellison 1
Dr. B. G. Herron 1

Hughes Research Laboratories
3011 Malibu Canyon Road
Malibu, CA 90265
Attn: Mr. J. H. Molitor 1
Dr. R. L. Poeschel 1
Dr. Jay Hyman 1
Mr. R. Vahrenkamp 1
Dr. J. R. Beattie 1
Dr. W. S. Williamson 1

IBM Corporation
Thomas J. Watson Research Center
P.O. Box 218
Yorktown Heights, NY 10598
Attn: Dr. Jerome J. Cuomo 1
Dr. James M. E. Harper 1

IBM East Fishkill
D/42K, Bldg. 300-40F
Hopewell Junction, NY 12533
Attn: Mr. James Winnard 1

Ion Beam Equipment, Inc.
P.O. Box 0
Norwood, NJ 07648
Attn: Dr. W. Laznovsky 1

Ion Tech, Inc.
P.O. Box 1388
1807 E. Mulberry
Fort Collins, CO 80522
Attn: Dr. Gerald C. Isaacson 1

Jet Propulsion Laboratory
4800 Oak Grove Drive
Pasadena, CA 91102
Attn: Dr. Kenneth Atkins 1
Technical Library 1
Mr. Eugene Pawlik 1
Mr. James Graf 1
Mr. Dennis Fitzgerald 1
Dr. Graeme Aston 1

Joint Institute for Laboratory Astrophysics
University of Colorado
Boulder, CO 80302
Attn: Dr. Gordon H. Dunn 1

Kyoto University
The Takagi Research Laboratory
Department of Electronics
Yoshidahonmachi Sakyo-ku
Kyoto 606,
JAPAN
Attn: Dr. Toshinori Takagi 1

Lawrence Livermore Laboratory
Mail Code L-437
P.O. Box 808
Livermore, CA 94550
Attn: Dr. Paul Drake 1

Lockheed Missiles and Space Company
Sunnyvale, CA 94088
Attn: Dr. William L. Owens
Propulsion Systems, Dept. 62-13 1
Mr. Carl Rudey 1

Massachusetts Institute of Technology
Room 13-3061
77 Massachusetts Avenue
Cambridge, MA 02139
Attn: Henry I. Smith 1

New Mexico State University
Department of Electrical and Computer Engr.
Las Cruces, NM 88003
Attn: Dr. Robert McNeil 1

Optic Electronics Corporation
11477 Pagemill Road
Dallas, TX 75243
Attn: Bill Hermann, Jr. 1

Physicon Corporation
221 Mt. Auburn Street
Cambridge, MA 02138
Attn: H. von Zweck 1

Princeton University
Princeton, NJ 08540
Attn: Mr. W. F. Von Jaskowsky 1
Dean R. G. Jahn 1
Dr. K. E. Clark 1

Research and Technology Division
Wright-Patterson AFB, OH 45433
Attn: (ADTN) Mr. Everett Bailey 1

Rocket Propulsion Laboratory
Edwards AFB, CA 93523
Attn: LKDA/Mr. Tom Waddell 1
LKDH/Dr. Robert Vondra 1

Royal Aircraft Establishment
Space Department
Farnborough, Hants
ENGLAND
Attn: Dr. D. G. Fearn 1

Sandia Laboratories
Mail Code 5743
Albuquerque, NM 87115
Attn: Mr. Ralph R. Peters 1

Tektronix, 50-324
P.O. Box 500
Beaverton, OR 97077
Attn: Curtis M. Haynes 1

Texas Instruments, Inc.
MS/34
P.O. 225012
Dallas, TX 75265
Attn: Larry Rehn 1

TRW Inc.
TRW Systems
One Space Park
Redondo Beach, CA 90278
Attn: Dr. M. Huberman 1
Mr. Sid Zafran 1

United Kingdom Atomic Energy Authority
Culham Laboratory
Abingdon, Berkshire
ENGLAND
Attn: Dr. P. J. Harbour 1
Dr. M. F. A. Harrison 1
Dr. T. S. Green 1

University of Tokyo
Department of Aeronautics
Faculty of Engineering
7-3-1, Hongo, Bunkyo-ku
Tokyo,
JAPAN
Attn: Prof. Itsuro Kimura 1

Veeco Instruments, Inc.
Terminal Drive
Plainview, NY 11803
Attn: Norman Williams 1

**End of Document**